NASA TN D-8

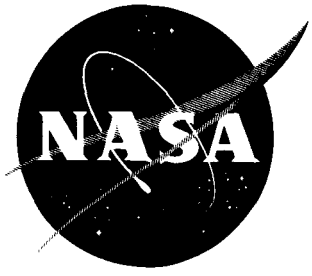

TECHNICAL NOTE

D-8

LAMINAR SKIN-FRICTION AND HEAT-TRANSFER PARAMETERS FOR A FLAT PLATE AT HYPERSONIC SPEEDS IN TERMS OF FREE-STREAM FLOW PROPERTIES

By James F. Schmidt

Lewis Research Center
Cleveland, Ohio

NATIONAL AERONAUTICS AND SPACE ADMINISTRATION

WASHINGTON September 1959

ERRATA

NASA TECHNICAL NOTE D-8

By James F. Schmidt

September 1959

E-280

Figure 1, page 25: The ordinate scale values should be .1, .2, .4, .6, .8, 1.0, and 2.0×10^{-6}. The ordinate scale should be "Reference density-viscosity parameter, $\rho^*\mu^*/P$, $lb^2/(ft^4)(sec)(atm)$."

NASA-Langley, 1962

Issued 4-20-62

NATIONAL AERONAUTICS AND SPACE ADMINISTRATION

TECHNICAL NOTE D-8

LAMINAR SKIN-FRICTION AND HEAT-TRANSFER PARAMETERS FOR A FLAT PLATE AT HYPERSONIC SPEEDS IN TERMS OF FREE-STREAM FLOW PROPERTIES

By James F. Schmidt

SUMMARY

In order to provide simple approximate design calculations, the skin-friction and heat-transfer parameters are presented in terms of the free-stream flow properties. A heat-transfer parameter based on the free-stream kinetic energy is introduced as a design simplification.

The skin-friction and heat-transfer parameters are calculated for a flat plate at angles of attack from 0° to 50° with equilibrium dissociation of air behind the shock wave and within the laminar boundary layer. These parameters are tabulated for wall temperatures between 1000° and 3000° R with free-stream velocities of 10,000 to 28,000 feet per second over an altitude range of 50,000 to 300,000 feet.

INTRODUCTION

The currently proposed hypersonic vehicles are usually conically shaped with a slight bluntness at the nose to reduce heating and with some fin arrangement for stability. This paper presents flat-plate friction and heat-transfer data for many of the hypersonic flight conditions of interest. Although conical shapes may not appear amenable to flat-plate analysis, Hantzsche and Wendt (ref. 1) have shown by a transformation of the laminar boundary-layer equations that flat-plate results can be applied to a cone (see appendix A for details). This, of course, is only applicable for a cone at zero angle of attack, thereby excluding all cross-flow problems.

At the present time many exact and approximate methods of calculating the laminar skin-friction and heat-transfer coefficients are available. However, these methods are usually very complex and require laborious mathematical operations to obtain even approximate results.

Moore (ref. 2) used a differential analyzer to calculate these coefficients based on the flow properties outside the boundary layer. An exact calculation, assuming a gas in chemical equilibrium, was made by Romig and Dore (ref. 3) with a differential analyzer. Eckert (ref. 4) used a semiempirical approach with a direct mathematical procedure for his calculations.

The preceding methods base their results either on the flow properties outside the boundary layer or on some reference-temperature flow properties. Unfortunately, dissociation of air at hypersonic speeds and high angles of attack makes it exceedingly difficult to obtain these flow properties. In order to eliminate this complication, the skin-friction and heat-transfer parameters are presented herein in terms of the free-stream flow properties. These parameters are calculated for the following range of free-stream conditions: altitude, 50,000 to 300,000 feet; velocity, 10,000 to 28,000 feet per second; angle of attack, 0° to 50°; and wall temperature, 1000° to 3000° R. Eckert's reference-enthalpy theory (ref. 4) of heat transfer is used for all calculations.

SYMBOLS

C_f	local skin-friction coefficient
C_q	local heat-energy coefficient
g	gravitational constant, ft/sec^2
h	static enthalpy, Btu/lb
h_c	heat-transfer coefficient based on enthalpy, lb/(sec)(sq ft)
J	mechanical equivalent of heat, ft-lb/Btu
K	adiabatic-wall enthalpy parameter
M	Mach number
P	static pressure, lb/sq ft
Pr	Prandtl number
q	heat transfer rate, Btu/(sec)(sq ft)
R	gas constant per unit weight of air (perfect gas)
Re	Reynolds number

r	recovery factor
St	Stanton number
T	static temperature, ^{o}R
V	velocity, ft/sec
x	distance along flat plate, ft
γ	ratio of specific heats (perfect gas)
μ	viscosity, lb/(ft)(sec)
ρ	density, lb/cu ft
τ_w	wall shearing stress, lb/sq ft

Subscripts:

a	adiabatic wall
w	wall
α	positive angle of attack
α=0	at zero angle of attack
δ	properties at edge of boundary layer
∞	free stream
2	behind shock

Superscripts:

*	reference enthalpy

The following sketches serve to define some of the symbols:

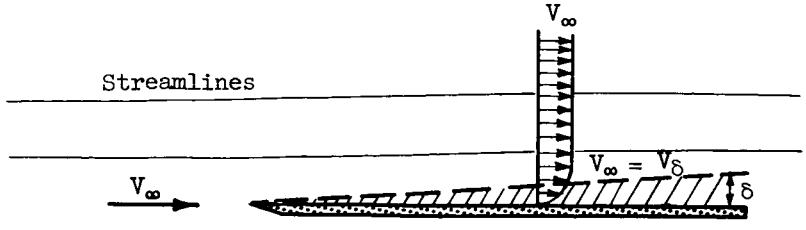

Note: Free-stream properties are equal to the properties at the edge of the boundary layer. $\infty = \delta$

Flat plate at zero angle of attack

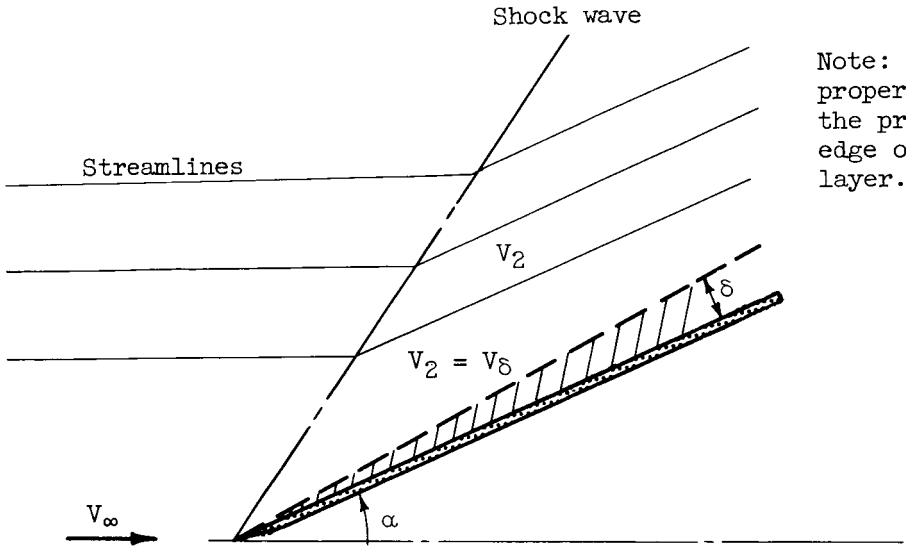

Note: Behind shock properties are equal to the properties at the edge of the boundary layer. 2 = δ

Flat plate at positive angle of attack

ANALYSIS

Continuum flow with equilibrium gas composition is assumed in this analysis based on references 5 to 7. At altitudes above 220,000 feet and for vehicle velocities less than 25,000 feet per second, the reaction rates are so slow that the flow approaches a frozen state (refs. 5 and 8). Also, for the same velocity range and altitude in excess of 240,000 feet the typical vehicle will enter slip flow (ref. 5). Although this assumption of continuum flow with equilibrium gas composition is invalid at the extreme conditions cited previously, the equilibrium results will provide a convenient reference for nonequilibrium analyses.

In addition to assuming continuum flow with equilibrium dissociation of air, the following assumptions are made:

1. The two-dimensional oblique shock is attached to the leading edge of the flat plate.

2. The flow properties behind the shock, assuming no viscous boundary-layer displacement interaction with the boundary layer, are equal to the properties at the edge of the boundary layer.

3. The static temperature and pressure of the air outside the boundary layer are constant.

4. The surface temperature along the plate is constant.

5. The modified Reynolds analogy is applicable for the considered flight conditions.

The assumption of no viscous boundary-layer displacement interaction is a good approximation for medium and large sharp-nosed cones and wedges, even at high Mach numbers (ref. 9). Also, the results of reference 9 show progressively better agreement with the inviscid prediction as the cone and wedge angle increase. This phenomenon of decreasing viscous boundary-layer displacement for increasing cone and wedge angles is caused by proportionately smaller changes in effective geometry due to boundary-layer growth for these thicker bodies. Hence, it is not surprising to find a large viscous boundary-layer displacement for a thin body such as a flat plate at zero angle of attack (refs. 9 and 10). This viscous boundary-layer displacement results in an induced pressure rise on the surface of the plate, cone, wedge, and so on. This induced pressure rise is further increased by leading-edge bluntness which is necessary for most current hypersonic vehicles (refs. 11 and 12). Reference 10 shows that a blunt leading-edge flat plate has a very large induced pressure rise, whereas a blunt-nosed cone and wedge have a significant but much smaller induced pressure rise (magnitude of cone pressure rise is in tenths of inviscid prediction compared with flat-plate pressure rise of 10 to 40). In fact, this induced pressure effect becomes smaller as the cone and wedge angle are increased.

In view of the preceding arguments, the viscous boundary-layer displacement is believed to have a negligible effect on the skin-friction and heat-transfer coefficients for medium and large, sharp-nosed cones and wedges. For the case of a flat plate (at zero angle of attack with a sharp or blunt leading-edge). Bogdonoff and Hammitt (refs. 13 to 16) have shown that the entire flow field is strongly affected by the viscous boundary-layer displacement. The viscous boundary-layer displacement for blunt-nosed cones and wedges is significant but is limited to a small region (usually not more than 5 nose diameters) from the nose of the cone or wedge (ref. 17)).

The 1956 ARDC atmosphere (ref. 18) is used in the oblique-shock calculations (refs. 19 and 20) with equilibrium dissociation as well as in the boundary-layer calculations. The thermodynamic and transport properties of air at high temperatures are obtained from a recent analysis (ref. 21).

All final equations are developed with the primary purpose of expressing the skin-friction and heat-transfer parameters in terms of the free-stream flow properties.

Skin-Friction Parameter

The local laminar shearing stress over an inclined flat plate can be defined in terms of free-stream or reference enthalpy flow properties by

$$\tau_w = C_{f,\infty} \frac{\rho_\infty V_\infty^2}{2g} = C_f^* \frac{\rho^* V_2^2}{2g} \tag{1}$$

where Eckert's definition of the reference skin friction coefficient C_f^* (ref. 4) is

$$C_f^* = 0.664 \left(\frac{\mu^*}{\rho^* V_2 x}\right)^{1/2} \tag{2}$$

By substituting equation (2) in equation (1) the local skin-friction parameter based on free-stream properties can be expressed as

$$C_{f,\alpha,\infty} (Re_\infty)^{1/2} = 0.664 \left(\frac{V_2}{V_\infty}\right)^{3/2} \left[\frac{(\rho^*\mu^*)_\alpha}{\rho_\infty \mu_\infty}\right]^{1/2} \tag{3}$$

where Re_∞ is the free-stream Reynolds number.

At zero angle of attack this skin-friction parameter reduces to

$$C_{f,\alpha=0,\infty} (Re_\infty)^{1/2} = 0.664 \left[\frac{(\rho^*\mu^*)_{\alpha=0}}{\rho_\infty \mu_\infty}\right]^{1/2} \tag{4}$$

where $\rho^*\mu^*$, the product of the reference density and viscosity is a function of the reference enthalpy and local surface pressure. The reference enthalpy for a laminar boundary layer is defined in appendix B. This function of the reference enthalpy and local surface pressure is derived in appendix C and plotted in figure 1.

The effect of angle of attack on the skin-friction parameter is easily represented by the ratio of the parameter at any angle of attack to its value at zero angle of attack. This ratio henceforth will be referred to as the skin-friction parameter ratio. Similarly, a heat-energy parameter ratio, defined in the same manner, indicates the effect of angle of attack on the heat-energy parameter.

By dividing equation (3) by equation (4), the skin-friction parameter ratio becomes

$$\frac{C_{f,\alpha,\infty} (Re_\infty)^{1/2}}{C_{f,\alpha=0,\infty} (Re_\infty)^{1/2}} = \left(\frac{V_2}{V_\infty}\right)^{3/2} \left[\frac{(\rho^*\mu^*)_\alpha}{(\rho^*\mu^*)_{\alpha=0}}\right]^{1/2} \tag{5}$$

where $\rho^*\mu^*$, which varies with angle of attack, is still only a function of the reference enthalpy and surface pressure.

Heat-Energy Parameter

The heat-transfer coefficient is often compared through a modified Reynolds analogy with a transfer of momentum across a boundary layer. However, this coefficient may also be compared through a modified Reynolds analogy with a transfer of energy (ref. 22) in a thermodynamic sense of heat; namely, a heat-energy coefficient. This heat-energy coefficient is defined in the following manner:

$$C_q = \frac{q}{\rho_\infty V_\infty^3/2gJ} \tag{6}$$

where q is the heat-transfer rate and the heat-energy coefficient C_q is a measure of the energy lost per unit wall surface divided by the energy of flow per cross-sectional area.

Since the heat-energy coefficient is based on the free-stream kinetic energy, it is extremely useful for aerodynamic heating problems and especially for reentry at high speeds. Actually, this heat-energy coefficient, which is based on the kinetic flow energy $\rho_\infty V_\infty^3/2g$, is very similar to the skin-friction coefficient, which is based on the dynamic flow pressure $\rho_\infty V_\infty^2/2g$.

The heat-transfer rate q can be written as

$$q = h_c(h_a - h_w) \tag{7}$$

where h_a is the adiabatic wall enthalpy, h_w is the wall enthalpy, and the heat-transfer coefficient h_c, based on enthalpy, may be written as

$$h_c = St^*\rho^*V_2 \tag{8}$$

where the Stanton number St^* with the modified Reynolds analogy is

$$St^* = \frac{C_f^*}{2}(Pr^*)^{-2/3} \tag{9}$$

With suitable rearrangement, equation (8) can be expressed in the following manner:

$$h_c = \frac{0.664}{2(Pr^*)^{2/3}} \frac{P_\infty V_\infty}{RT_\infty (Re_\infty)^{1/2}} \left[\frac{(\rho^*\mu^*)_\alpha}{\rho_\infty \mu_\infty} \frac{V_2}{V_\infty}\right]^{1/2} \tag{10}$$

(See appendix D for the derivation of eq. 10.)

The enthalpy difference $h_a - h_w$ of equation (7) can be expressed conveniently by the following adiabatic-wall enthalpy parameter:

$$K_\alpha = \frac{h_a - h_w}{h_\infty} \tag{11}$$

(The adiabatic-wall enthalpy parameter is derived in appendix E.) By substituting equations (10) and (11) in equation (7) and reducing, the heat-transfer rate becomes

$$q = \frac{0.664}{2(Pr^*)^{2/3}} \left(\frac{\gamma_\infty}{\gamma_\infty - 1}\right) \frac{K_\alpha (P_\infty V_\infty)}{J(Re_\infty)^{1/2}} \left[\frac{(\rho^*\mu^*)_\alpha}{\rho_\infty \mu_\infty} \frac{V_2}{V_\infty}\right]^{1/2} \tag{12}$$

The product of the free-stream pressure and velocity $P_\infty V_\infty$ can be expressed as a function of the energy of flow per cross-sectional area. This relation is conveniently given by the following equation:

$$P_\infty V_\infty = \frac{\rho_\infty V_\infty^3 / 2g}{\gamma_\infty M_\infty^2 / 2} \tag{13}$$

The heat-energy parameter can now be obtained by combining equations (13) and (12) with equation (6). At zero angle of attack this parameter reduces to

$$C_{q,\alpha=0} (Re_\infty)^{1/2} = \frac{0.664}{(Pr^*)^{2/3}} \frac{K_{\alpha=0}}{(\gamma_\infty - 1)M_\infty^2} \left[\frac{(\rho^*\mu^*)_{\alpha=0}}{\rho_\infty \mu_\infty}\right]^{1/2} \tag{14}$$

The heat-energy parameter ratio, defined in the same manner as the skin-friction parameter ratio, is simply

$$\frac{C_{q,\alpha} (Re_\infty)^{1/2}}{C_{q,\alpha=0} (Re_\infty)^{1/2}} = \frac{K_\alpha}{K_{\alpha=0}} \left(\frac{V_2}{V_\infty}\right)^{1/2} \left[\frac{(\rho^*\mu^*)_\alpha}{(\rho^*\mu^*)_{\alpha=0}}\right]^{1/2} \tag{15}$$

The evaluation of $\rho^*\mu^*$ is exactly the same as for the skin-friction parameter.

DISCUSSION

The calculation procedure used for obtaining the values in the tables is explained in appendix F. All the calculations are based on the 1956 ARDC model atmosphere (ref. 18). The variation of the atmospheric pressure and temperature with altitude is plotted in figure 2.

Skin-Friction Parameter

Effect of altitude. - From figure 5 the effect of altitude on the skin-friction parameter at zero angle of attack is very slight (maximum variation within 4.0 percent). At velocities below 16,000 feet per second this variation is predominantly a function of the atmospheric temperature change with altitude. This temperature change with altitude is clearly shown in figure 2. For the higher velocities there is a dissociation effect mixed in with the previously mentioned temperature-change effect. The effect of dissociation on the skin-friction parameter at zero angle of attack is shown in figure 5 to cause a steady increase as a function of velocity. At 20,000 feet per second this effect results in approximately a 2.0 percent increase in the skin-friction parameter. Figure 4 shows that the effect of altitude on the skin-friction parameter ratio at large angles of attack is large (maximum variation within 27 percent). This effect is also caused more by the atmospheric temperature change with altitude than by dissociation (note the largest variation at 150,000 ft where the temperature-change effect is most significant).

The results shown by the dashed lines of figure 5 may be in error because the conditions of continuum flow with equilibrium dissociation are probably not satisfied at the extreme flight conditions (refs. 5 and 7). Also, the data indicated by the dashed lines are slightly beyond the range of the transport properties presented in reference 21. However, as stated in the analysis, the equilibrium results as indicated by the dashed lines are believed to provide a convenient reference for nonequilibrium analyses.

Effect of angle of attack. - Figure 6 shows that the skin-friction parameter ratio increases steadily with angle of attack until it reaches a maximum at approximately 35°. At larger angles of attack this parameter ratio begins to decline and then steadily decreases until the maximum angle is reached. This behavior is believed to be caused by the extreme reduction of velocity across the shock wave, especially since the velocity decrease is most prominent at large angles of attack.

Effect of wall temperature. - Figure 7 shows that the skin-friction parameter at zero angle of attack decreases almost linearly with increasing wall temperature at all altitudes other than 50,000 feet. The reason for this nonlinear effect at 50,000 feet is not presently apparent. At the lower wall temperatures (500° to 2000° R) there seems to be a discrepancy in the curves for velocities of 20,000 and 22,000 feet per second, especially at the higher altitudes (200,000 to 300,000 ft). The reason for this is uncertain, but since the discrepancy becomes steadily greater with altitude a possible pressure effect is suggested. At angle of attack, even at large angles of attack, the skin-friction parameter ratio is approximately independent of the wall temperature up to 2000° R for the complete velocity and altitude range (e.g., fig. 8).

Comparison of results with other solutions. - In figure 9 the present solution of this paper for the skin-friction parameter at zero angle of attack is compared with solutions by Romig and Dore (ref. 3), Moore (ref. 2), and Young and Janssen (ref. 23). The present solution agrees very well (within 2.0 percent) with the methods of Romig and Dore, and Moore. These two methods also assume equilibrium dissociation in the boundary-layer calculations. The method of Young and Janssen, which assumes a perfect gas composition, does not compare quite as favorably (within 5.0 percent) with the present solution. These comparisons are not exactly correct since, as listed in figure 9, the wall temperatures and initial temperatures of the air for the various solutions are slightly different. However, these variations are small and result in a negligible effect on the skin-friction parameter.

Heat-Energy Parameter

Effect of altitude. - The effect of altitude on the heat-energy parameter at zero angle of attack (fig. 10) is small (within 5 percent). As before, this altitude effect is caused more by the atmospheric temperature change with altitude than by dissociation. The effect of dissociation on the heat-energy parameter is shown in figure 11 to cause a steady increase as a function of velocity. At 20,000 feet per second this effect results in approximately a 2.0 percent increase in the heat-energy parameter. Figure 12 shows that the effect of altitude on the heat-energy parameter ratio is large (maximum variation of 22.0 percent at $\alpha = 45^{\circ}$).

Effect of angle of attack. - Figure 13 shows that the heat-energy parameter ratio increases steadily with angle of attack up to approximately 45°. At this point the curves appear to flatten out and are essentially constant until the maximum angle of attack (approx. 50°) is reached.

Effect of wall temperature. - From figure 14 it can be seen that the wall temperature has a large almost-linear effect (up to 80 percent) on the heat-energy parameter at zero angle of attack, especially at the lower velocities. This effect (same as for the skin-friction parameter) becomes nonlinear only at an altitude of 50,000 feet for wall temperatures above 2000° R. Similar to the skin-friction parameter, there appears to be a discrepancy in the curves for velocities of 20,000 and 22,000 feet per second, especially at the high altitudes. Again the reason for this is uncertain, but the discrepancy seems to be some type of pressure effect with altitude (maybe a dissociation effect, which is nullified at the higher velocities and does not exist at the lower velocities). At positive angles of attack the heat-energy parameter ratio is essentially independent of wall temperature up to 2000° R over the complete velocity and altitude range (e.g., fig. 16).

Comparison of results with other solutions. - In figure 15 the present solution for the heat-transfer rate is compared with the method of Romig and Dore (ref. 3). The method of Romig and Dore is an exact solution of the laminar boundary layer for highly-dissociated stream properties outside the boundary layer. These dissociated stream properties are substituted into the present solution for an equivalent comparison. This comparison is quite favorable (within 6.0 percent), even under conditions of extreme dissociation.

CALCULATIONS AT WALL TEMPERATURES OTHER THAN 1000° R

Figures 7 and 14 give the skin-friction and heat-energy parameters, respectively, at zero angle of attack for wall temperatures from 500° to 3000° R. From figures 8 and 16 it is clearly seen that the skin-friction and heat-energy parameter ratios are independent of wall temperature up to 2000° R. Therefore, the skin-friction and heat-energy parameters at any positive angle of attack can be determined for wall temperatures between 500° and 2000° R. This parameter at positive angles of attack is obtained by selecting the appropriate parameter at zero angle of attack from figures 7 or 14 (determined by free-stream conditions) and multiplying the result by the appropriate parameter ratio from figures 6 or 13 (also determined by free-stream conditions).

CONCLUDING REMARKS

It has been found that accurate estimation of the transport properties, especially at high temperatures, is the most important factor in calculating the skin friction and heat-energy parameters. In fact, the larger variations in a comparison of calculation methods for heat transfer can usually be attributed to the differences in evaluation of the transport properties. However, accurate evaluation of the transport properties at very high temperatures is extremely difficult, especially over a wide range of pressures. Therefore, in order to provide simple approximate design calculations, the skin-friction and heat-energy parameters are presented in terms of the free-stream flow properties. These simplified equations can easily be applied to reentry drag and heat-transfer problems.

Lewis Research Center
National Aeronautics and Space Administration
Cleveland, Ohio, February 6, 1959

APPENDIX A

APPLICATION TO CONICAL SHAPES

As stated in the INTRODUCTION, flat-plate skin-friction and heat-transfer results can be applied to a cone at zero angle of attack by a transformation of the laminar boundary-layer equations (ref. 1). This transformation requires that the skin-friction and heat-energy parameters for a flat plate be multiplied by $\sqrt{3}$ to obtain these parameters for a cone at the same distance from the nose as from the leading edge. Also, the local external conditions at the edge of the boundary layer for a cone must be the same as for the flat plate.

It is well known from classical aerodynamics that the air properties acting on a cone surface are greatly different from the properties acting on a two-dimensional wedge surface for the same flight conditions and equal cone and wedge angles. This difference is caused by the continuous compression of the air between the conical shock wave and the cone surface. However, for high flight speeds and large cone angles, the actual compression of the air behind the conical shock wave is extremely small. In fact, Romig (ref. 24) has shown by an exact calculation method that the air properties acting on a wedge surface are almost equal to the properties acting on a cone surface with the same shock angle, provided that the flight velocity is 10,000 feet per second or greater and that the cone semivertex angle is at least 15°. For precise calculations Romig has developed an equation that relates the cone semivertex angle to the shock-wave angle in terms of the free-stream Mach number and pressure. This equation is defined as

$$M_{\infty} \sin \theta = A + BM_{\infty} \sin \sigma \tag{A1}$$

where θ is the shock wave angle, σ is the cone semivertex angle, and A and B are functions of pressure.

$$A = 0.39 - 0.01 \log P_{\infty} \tag{A2}$$

$$B = 1.03 - 0.005 \log P_{\infty} \tag{A3}$$

where P_{∞} is the free-stream pressure in atmospheres. Equations (A1), (A2), and (A3) are appropriate for the following range of conditions: pressure, 10^{-1} to 10^{-4} atmospheres; velocity, 10,000 to 32,000 feet per second; cone semivertex angle, 20° to 50°; and the combined velocity and cone semivertex angle requirement, $M_{\infty} \sin \sigma \geqq 6$.

From equation (A1) flat-plate (at angle of attack) or two-dimensional, wedge surface properties can be directly related to cone surface properties. Once the shock wave angle is calculated from equation (A1), oblique-shock-wave data can be used to obtain the correct wedge angle or surface properties for the arbitrarily chosen cone semivertex angle at the same flight conditions.

APPENDIX B

THE REFERENCE ENTHALPY

Eckert's reference enthalpy (ref. 4) may be written as

$$h^* = \frac{1}{2}(h_2 + h_w) + 0.22\, r\left(\frac{V_2^2}{2gJ}\right) \tag{B1}$$

where r is the recovery factor and $V_2^2/2gJ$ can be expressed in terms of the energy equation per unit mass

$$\frac{V_2^2}{2gJ} = h_\infty - h_2 + \frac{V_\infty^2}{2gJ} \tag{B2}$$

By substituting equation (B2) in (B1) and rearranging terms, the reference enthalpy becomes

$$\left(\frac{h^*}{100}\right)_\alpha = \frac{h_\infty}{100}\left\{\left(\frac{1}{2} - 0.22\, r\right)\frac{h_2}{h_\infty} + \frac{1}{2}\frac{h_w}{h_\infty} + 0.22\, r\left[1 + \left(\frac{\gamma_\infty - 1}{2}\right)M_\infty^2\right]\right\} \tag{B3}$$

where h_2/h_∞, the enthalpy ratio across the shock wave, is obtained from the shock calculations of reference 19.

At zero angle of attack, equation (B3) reduces to

$$\left(\frac{h^*}{100}\right)_{\alpha=0} = \frac{h_\infty}{100}\left\{\left(\frac{1}{2} - 0.22\, r\right) + \frac{1}{2}\frac{h_w}{h_\infty} + 0.22\, r\left[1 + \left(\frac{\gamma_\infty - 1}{2}\right)M_\infty^2\right]\right\} \tag{B4}$$

where r, the recovery factor for a laminar boundary layer, is

$$r = (Pr^*)^{1/2} \tag{B5}$$

From the transport properties of reference 21 the Prandtl number to be evaluated at the reference enthalpy, is assumed constant at 0.71. Although this Prandtl number will vary to a sizable degree (0.58 to 0.77) over a wide temperature range (500° to 5500° K), this change has a relatively small effect on the desired parameters. This effect results in a maximum error of only 2.5 percent on the final parameters when the extreme values of the Prandtl number are compared.

APPENDIX C

EVALUATION OF $\rho^*\mu^*$

Reference 21 presents recent tabulated values for the thermodynamic and transport properties of high-temperature air. This reference assumes equilibrium dissociation of air which, as discussed previously, is a basic assumption of this analysis. From reference 21 the thermodynamic properties of high-temperature air have an accuracy of the order of 2 to 5 percent. For the range of flight conditions considered the transport properties of reference 21 have an approximate accuracy of the order of 5 to 20 percent. From these tabulated data the reference density and viscosity $\rho^*\mu^*$ can be expressed as a function of only the reference enthalpy and surface pressure (fig. 1). This functional approximation for $\rho^*\mu^*$ has a maximum error of ± 4 percent compared with the results of reference 21. These functions, which are applicable for a pressure range of 10 to 0.0001 atmospheres, are presented in the following table:

Reference enthalpy parameter, $h^*/100$, Btu/lb	Product of reference density and viscosity, $\rho^*\mu^*$, $lb^2/(ft^4)(sec)\times 10^6$
1 to 8	$1.1\left(\frac{h^*}{100}\right)^{-0.382} P^{1.0}$
8 to 25	$1.1\left(\frac{h^*}{100}\right)^{-0.382} P^{0.9925} + A$
25 to 50	$1.1\left(\frac{h^*}{100}\right)^{-0.382} P^{0.9925}$
50 to 150	$0.84\left(\frac{h^*}{100}\right)^{-0.313} P^{0.9925}$
Where $A = 0.4975\ (P^{0.9925} - P^{1.0})\ \frac{\left(\frac{h^*}{100} - 25\right)}{17}$	

*Pressure P is in atmospheres.

APPENDIX D

DERIVATION OF THE HEAT-TRANSFER COEFFICIENT

The heat-transfer coefficient based on enthalpy is

$$h_c = St^* \rho^* V_2 \tag{D1}$$

where the Stanton number St^* with the Modified Reynolds Analogy is

$$St^* = \frac{C_f^*}{2} (Pr^*)^{-2/3} \tag{D2}$$

By substituting equation (D2) in (D1), the heat-transfer coefficient becomes

$$h_c = \frac{C_f^* \rho^* V_2}{2(Pr^*)^{2/3}} \tag{D3}$$

With the substitution of the skin-friction coefficient, equation (2), the laminar heat-transfer coefficient is

$$h_c = \frac{0.664}{2(Pr^*)^{2/3}} \left(\frac{\rho^* \mu^* V_2}{x} \right)^{1/2} \tag{D4}$$

By rearranging equation (D4), the laminar heat-transfer coefficient is reduced to equation (8)

$$h_c = \frac{0.664}{2(Pr^*)^{2/3}} \left[\frac{(\rho^* \mu^*)(\rho_\infty V)^2 V_2}{\left(\frac{\rho_\infty V_\infty x}{\mu_\infty} \right) \rho_\infty \mu_\infty V_\infty} \right]^{1/2} = \frac{0.664}{2(Pr^*)^{2/3}} \frac{P_\infty V_\infty}{RT_\infty (Re_\infty)^{1/2}} \left(\frac{V_2}{V_\infty} \frac{\rho^* \mu^*}{\rho_\infty \mu_\infty} \right)^{1/2} \tag{D5}$$

APPENDIX E

THE ADIABATIC-WALL ENTHALPY PARAMETER

The adiabatic-wall enthalpy parameter is defined by

$$K_\alpha = \frac{h_a - h_w}{h_\infty} \tag{E1}$$

where h_a, the adiabatic wall enthalpy is

$$h_a = h_2 + r\frac{V_2^2}{2gJ} \tag{E2}$$

By combining equations (B2) and (E2) with (E1) and simplifying, the adiabatic-wall enthalpy parameter can be expressed by

$$K_\alpha = (1 - r)\frac{h_2}{h_\infty} + r\left[1 + \left(\frac{\gamma_\infty - 1}{2}\right)M_\infty^2\right] - \frac{h_w}{h_\infty} \tag{E3}$$

At zero angle of attack equation (E3) reduces to

$$K_{\alpha=0} = (1 - r) + r\left[1 + \left(\frac{\gamma_\infty - 1}{2}\right)M_1^2\right] - \frac{h_w}{h_\infty} \tag{E4}$$

where r, the recovery factor, is defined in appendix B.

APPENDIX F

CALCULATION PROCEDURE

Skin-Friction Parameter

The skin-friction parameter at zero angle of attack is determined from equation (4) with the reference density and viscosity evaluated by the proper function of the reference enthalpy and surface pressure in the table in appendix C. Therefore, the reference enthalpy, which is defined in appendix B must first be calculated before the reference density and viscosity can be determined. As stated in the DISCUSSION, the atmospheric properties of air are obtained from reference 18. (The variation of temperature and pressure with altitude is shown in fig. 2.) The skin-friction parameter is tabulated in table I for a wall temperature of 1000° R with free-stream velocities of 10,000 to 28,000 feet per second over an altitude range of 50,000 to 300,000 feet. In addition, this parameter is tabulated in table III for wall temperatures up to 3000° R with the same velocity and altitude range as previously given.

At positive angles of attack the skin-friction parameter ratio is obtained from equation (5) with the reference density and viscosity evaluated by the same procedure as above. In this case, however, there is an oblique shock wave attached to the flat plate and the velocity ratio across the shock wave is obtained from the shock-wave calculations of reference 19. The skin-friction parameter ratio for a wall temperature of 1000° R is tabulated in table I with angles of attack up to 50° for the preceding altitude and velocity range.

Heat-Energy Parameter

The heat-energy parameter at zero angle of attack is determined from equation (14) with the reference density and viscosity evaluated in the same manner as for the skin-friction parameter. The adiabatic-wall enthalpy parameter used in equation (14) is calculated from appendix E. This heat-energy parameter is tabulated in table II for a wall temperature of 1000° R with the previously given velocity and altitude range. Also, this parameter is tabulated in table IV for wall temperatures up to 3000° R with the same velocity and altitude range.

The heat-energy parameter ratio is calculated from equation (15) with the reference density and viscosity evaluated by the same procedure as for the skin-friction parameter ratio. Likewise, the velocity ratio across the shock wave and the adiabatic-wall enthalpy parameter are determined by the same procedure as above. The heat-energy parameter ratio for a wall temperature of 1000° R is tabulated in table II with angles of attack up to 50° for the previous velocity and altitudes range.

REFERENCES

1. Hantzsche, W. and Wendt, H.: The Laminar Boundary Layer on a Circular Cone in Supersonic Stream. Reps. and Trans. No. 276, British M.A.P., Aug. 1946.

2. Moore, L. L.: A Solution of the Laminar Boundary-Layer Equations for a Compressible Fluid with Variable Properties, Including Dissociation. Jour. Aero. Sci., vol. 19, no. 8, Aug. 1952, pp. 505-518.

3. Romig, Mary F., and Dore, F. J.: Solutions of the Compressible Laminar Boundary Layer Including the Case of a Dissociated Free Stream. Rep. ZA-7-012, San Diego Div., Convair, Aug. 4, 1954.

4. Eckert Ernst R. G.: Survey on Heat Transfer at High Speeds. Tech. Rep. 54-70, Aero. Res. Lab., WADC, Apr. 1954. (Contract AF 33(616)-2214.)

5. Hansen, C. Frederick, and Heims, Steve P.: A Review of the Thermodynamic, Transport, and Chemical Reaction Rate Properties of High-Temperature Air. NACA TN 4359, 1958.

6. Blackman, Vernon: Vibrational Relaxation in Oxygen and Nitrogen. Jour. Fluid Mech., vol. 1, pt. 1, May 1956, pp. 61-85.

7. Camac, M., et. al.: Chemical Relaxation in Air, Oxygen and Nitrogen. Preprint No. 802, Inst. Aero. Sci., 1958.

8. Rose, P. H.: Physical Gas Dynamics Research at the AVCO Research Laboratory. Res. Rep. No. 9, AVCO Res. Lab., May 1957.

9. Erickson, Wayne D.: Study of Pressure Distributions on Simple Sharp-Nosed Models at Mach Numbers from 16 to 18 in Helium Flow. NACA TN 4113, 1957.

10. Bertram, Mitchel H., and Henderson, Arthur, Jr.: Effects of Boundary-Layer Displacement and Leading-Edge Bluntness on Pressure Distribution, Skin Friction, and Heat Transfer of Bodies at Hypersonic Speeds. NACA TN 4301, 1958.

11. Allen, H. Julian, and Eggers, A. J., Jr.: A Study of the Motion and Aerodynamic Heating of Missiles Entering the Earth's Atmosphere at High Supersonic Speeds. NACA TN 4047, 1957. (Supersedes NACA RM A53D28.)

12. Eggers, Alfred J., Jr., Allen, H. Julian, and Neice, Stanford E.: A Comparative Analysis of the Performance of Long-Range Hypervelocity Vehicles. NACA TN 4046, 1957. (Supersedes NACA RM A54L10.)

13. Hammitt, A. G., Vas, I. E., and Bogdonoff, S. M.: Leading Edge Effects on the Flow Over a Flat Plate at Hypersonic Speeds. Rep. No. 326, Dept. Aero. Eng., Princeton Univ., Sept. 1955.

14. Hammitt, Andrew G.: The Hypersonic Viscous Effect on a Flat Plate with Finite Leading Edge. Rep. No. 378, WADC TN 57-105, Dept. Aero. Eng., Princeton Univ., Mar. 1957.

15. Bogdonoff, S. M., and Vas, I. E.: Preliminary Study of the Flow Over a Blunt Flat Plate at Various Angles of Attack at M = 13.3. I - Studies of Flat and Hemi-Cylindrical Leading Edges. Bell Aircraft Corp., May 15, 1956.

16. Bogdonoff, S. M., and Vas, I. E.: Preliminary Study of the Flow Over a Blunt Flat Plate at Various Angles of Attack at M = 13.3. II - Study of an Elliptical Leading Edge. Bell Aircraft Corp., Oct. 1, 1956.

17. Bogdonoff, S. M., and Vas, I. E.: Investigation of the Flow About Bodies of Revolution at Mach Numbers from 12 to 19. I - Preliminary Results of a Series of Forebodies at Zero Angle of Attack. Tech. Rep. No. 5, Gruen Appl. Sci. Labs., Oct. 1956. (Contract SDP-40121.)

18. Minzner, R. A., and Ripley, W. S.: The ARDC Model Atmosphere, 1956. TN 56-204, AF Cambridge Res. Center, Air Res. and Dev. Command, Dec. 1956.

19. Aerodynamics Section of Douglas Aircraft Company: Normal and Oblique Shock Characteristics at Hypersonic Speeds. Eng. Rep. No. LB-25599, ARDC-TR-57-184, Douglas Aircraft Co., Inc., Dec. 31, 1957.

20. Moeckel, W. E.: Oblique-Shock Relations at Hypersonic Speeds for Air in Chemical Equilibrium. NACA TN 3895, 1957.

21. Hansen, C. Frederick: Approximations for the Thermodynamic and Transport Properties of High-Temperature Air. NACA TN 4150, 1958.

22. Bakhmeteff, Boris A.: The Analogy Between Fluid Friction and Heat Transfer. Trans. ASME, vol. 62, no. 7, Oct. 1940, pp. 551-553.

23. Young, George B. W., and Janssen, Earl: The Compressible Boundary Layer. Jour. Aero. Sci., vol. 19, no. 4, Apr. 1952, pp. 229-236.

E-280

CH-3 back

24. Romig, Mary F.: Conical Flow Parameters for Air in Dissociation Equilibrium: Final Results. Res. Note 14, Sci. Res. Lab., Convair, Jan. 1958.

TABLE I. - SKIN-FRICTION PARAMETER

[Wall static temperature, T_w, 1000° R.]

Velocity, V, ft/sec	Skin-friction parameter, $C_{f,\alpha=0,\infty}(Re_\infty)^{\frac{1}{2}}$	Skin-friction parameter ratio, $C_{f,\alpha,\infty}(Re_\infty)^{1/2} / C_{f,\alpha=0,\infty}(Re_\infty)^{1/2}$									
		Angle of attack, α, deg									
	0	5	10	15	20	25	30	35	40	45	50
					Altitude, 50,000 ft						
10,000	0.5122	1.738	2.564	3.384	4.060	4.433	4.563	4.386	4.041	3.477	2.244
12,000	.4870	1.989	3.020	4.034	4.675	5.287	5.490	5.504	5.124	4.526	3.395
14,000	.4649	2.177	3.456	4.668	5.537	6.081	6.284	6.250	5.995	5.302	4.354
16,000	.4459	2.436	3.849	5.283	6.293	6.997	7.296	7.312	6.828	6.170	4.934
18,000	.4292	2.578	4.239	5.791	6.870	7.694	8.122	8.162	7.816	6.955	5.597
20,000	.4147	2.718	4.627	6.356	7.543	8.543	9.018	8.987	8.578	7.910	6.334
22,000	.4019	2.879	5.035	6.942	8.221	9.309	9.827	9.825	9.427	8.535	7.128
24,000	.3907	3.079	5.436	7.503	8.996	10.14	10.70	10.76	10.27	9.259	-----
26,000	.3802	3.277	5.852	8.144	9.724	10.93	11.57	11.70	11.09	-----	-----
28,000	.3702	3.487	6.280	8.478	10.35	11.71	12.55	12.58	12.11	-----	-----
					Altitude, 100,000 ft						
10,000	0.5148	1.728	2.517	3.305	3.844	4.386	4.422	4.392	4.219	3.377	2.197
12,000	.4896	1.998	2.987	3.605	4.507	5.071	5.266	5.186	4.861	4.252	3.344
14,000	.4676	2.221	3.377	4.417	5.159	5.837	6.148	6.255	5.852	5.234	4.241
16,000	.4486	2.434	3.788	5.042	6.028	6.698	6.993	7.044	6.756	6.085	5.009
18,000	.4324	2.547	3.908	5.635	6.669	7.443	7.878	7.968	7.638	6.889	5.693
20,000	.4184	2.695	4.456	6.223	7.368	8.286	8.732	8.687	8.205	7.477	6.318
22,000	.4063	2.797	4.806	6.717	8.024	8.960	9.492	9.514	9.122	8.210	6.959
24,000	.3958	2.992	5.255	7.127	8.631	9.775	10.36	10.45	9.924	9.056	7.744
26,000	.3859	3.186	5.658	7.737	9.390	10.54	11.19	11.30	10.91	9.890	8.538
28,000	.3758	3.386	6.100	8.338	10.11	11.32	12.01	12.12	11.75	10.85	9.413
					Altitude, 150,000 ft						
10,000	0.5221	1.656	2.399	3.039	3.527	3.980	4.016	4.086	3.599	2.880	2.324
12,000	.4969	1.866	2.731	3.576	4.163	4.678	4.870	4.718	4.503	3.928	3.320
14,000	.4750	2.072	3.085	4.116	4.790	5.501	5.771	5.665	5.370	4.824	4.004
16,000	.4562	2.275	3.470	4.576	4.554	6.279	6.511	6.525	6.136	5.590	4.641
18,000	.4402	2.415	3.678	5.084	6.180	6.978	7.262	7.327	7.040	6.382	5.306
20,000	.4265	2.526	4.010	5.549	6.763	7.626	8.089	7.925	7.604	6.955	5.928
22,000	.4149	2.620	4.340	6.108	7.385	8.236	8.654	8.765	8.406	7.725	6.651
24,000	.4051	2.792	4.733	6.579	7.956	9.013	9.448	9.569	9.242	8.472	7.345
26,000	.3954	2.970	5.084	7.037	8.565	9.655	10.29	10.40	10.05	9.218	8.111
28,000	.3851	3.149	5.418	7.591	9.259	10.48	11.11	11.22	10.86	10.07	8.864
					Altitude, 200,000 ft						
10,000	0.5181	1.695	2.496	3.096	3.124	4.068	4.398	4.177	3.805	3.398	2.692
12,000	.4928	1.957	2.830	3.868	4.442	4.619	5.094	5.172	4.886	4.446	3.517
14,000	.4711	2.191	3.277	4.442	5.176	5.773	5.916	5.916	5.680	5.153	4.259
16,000	.4522	2.196	3.673	4.822	5.784	6.512	6.811	6.876	6.573	5.935	4.976
18,000	.4369	2.405	3.819	5.336	6.463	7.207	7.658	7.733	7.422	6.764	5.684
20,000	.4238	2.600	4.460	6.145	7.069	7.943	8.482	8.403	8.034	7.385	6.273
22,000	.4127	2.777	4.642	6.458	7.701	8.490	9.037	9.202	8.879	8.171	7.084
24,000	.4037	2.942	5.013	6.823	8.649	9.359	9.919	9.986	9.702	8.970	7.830
26,000	.3945	3.091	5.311	7.385	8.965	10.14	10.72	10.81	10.46	9.700	8.566
28,000	.3841	3.246	5.802	7.898	9.587	10.83	11.54	11.70	11.49	10.63	9.430
					Altitude, 250,000 ft						
10,000	0.5092	1.808	2.688	3.535	4.074	4.588	4.816	4.771	4.470	4.060	3.150
12,000	.4841	2.088	3.168	4.217	4.992	5.591	5.887	5.773	5.471	5.042	4.121
14,000	.4625	2.285	3.628	4.696	5.697	6.369	6.658	6.706	6.497	5.963	5.111
16,000	.4441	2.465	4.042	5.369	6.474	7.234	7.713	7.824	7.505	6.861	5.964
18,000	.4289	2.672	4.454	5.849	7.234	8.170	8.672	8.826	8.506	7.801	6.692
20,000	.4165	2.781	4.937	6.712	7.991	9.047	9.657	9.523	9.107	8.351	7.221
22,000	.4064	2.993	5.109	7.112	8.646	9.684	10.32	10.41	10.09	9.291	8.157
24,000	.3983	3.201	5.698	7.763	9.401	10.56	11.27	11.42	11.04	10.24	8.973
26,000	.3900	3.409	6.115	8.357	10.15	11.51	12.18	12.36	11.99	11.13	9.887
28,000	.3796	3.656	6.580	8.980	10.92	12.29	13.11	13.50	13.04	12.14	10.79
					Altitude, 300,000 ft						
10,000	0.5100	-----	-----	-----	------	------	------	------	------	------	------
12,000	.4847	-----	-----	-----	------	------	------	------	------	------	------
14,000	.4629	2.302	3.586	4.709	5.716	6.405	6.762	6.807	6.541	6.111	5.168
16,000	.4449	2.469	4.051	5.439	6.549	7.332	7.759	7.870	7.567	7.054	6.048
18,000	.4303	2.604	4.469	6.133	7.313	8.213	8.741	8.790	8.628	7.918	6.767
20,000	.4185	2.783	4.574	6.662	8.092	9.099	9.758	9.592	9.170	8.510	7.382
22,000	.4097	2.994	5.289	7.205	8.806	9.740	10.36	10.46	10.16	9.427	8.231
24,000	.4020	3.208	5.783	7.833	9.384	10.54	11.23	11.38	11.13	10.33	9.177
26,000	.3941	3.414	6.123	8.434	10.19	11.50	12.35	12.38	12.11	11.32	10.06
28,000	.3838	3.630	6.466	8.874	10.92	12.45	13.17	13.35	13.07	12.25	10.92

TABLE II. - HEAT-ENERGY PARAMETER

[Wall static temperature, T_w, 1000° R.]

Velocity, V, ft/sec	Heat-energy parameter, $C_{q,\alpha=0}(Re_\infty)^{\frac{1}{2}}$	Heat-energy parameter ratio, $C_{q,\alpha}(Re_\infty)^{1/2} / C_{q,\alpha=0}(Re_\infty)^{1/2}$									
		Angle of attack, α, deg									
	0	5	10	15	20	25	30	35	40	45	50
Altitude, 50,000 ft											
10,000	0.2478	1.765	2.666	3.664	4.653	5.475	6.193	6.771	7.033	7.239	6.777
12,000	.2424	2.017	3.138	4.367	5.463	6.505	7.227	7.996	8.440	8.701	8.464
14,000	.2353	2.205	3.570	5.045	6.327	7.326	8.227	9.000	9.659	9.957	9.958
16,000	.2282	2.466	3.986	5.702	7.168	8.425	9.495	10.41	10.95	11.35	11.20
18,000	.2213	2.607	4.383	6.220	7.720	9.176	10.44	11.45	12.25	12.67	12.57
20,000	.2149	2.746	4.778	6.816	8.493	10.20	11.57	12.62	13.41	13.90	13.91
22,000	.2091	2.906	5.179	7.440	9.206	11.05	12.55	13.74	14.70	15.26	15.31
24,000	.2038	3.106	5.611	8.039	10.06	12.01	13.63	14.98	16.02	16.59	-----
26,000	.1988	3.306	6.037	8.683	10.85	12.92	14.70	16.21	17.30	-----	-----
28,000	.1939	3.516	6.476	9.032	11.49	13.77	15.86	17.41	18.69	-----	-----
Altitude, 100,000 ft											
10,000	0.2501	1.757	2.620	3.596	4.370	5.399	5.950	6.523	6.980	6.978	6.560
12,000	.2444	2.029	3.111	3.883	5.178	6.191	6.982	7.599	8.059	8.254	8.157
14,000	.2372	2.252	3.506	4.745	5.896	7.079	8.040	8.898	9.409	9.725	9.680
16,000	.2299	2.466	3.928	5.393	6.817	8.038	9.094	9.974	10.65	11.04	11.04
18,000	.2233	2.577	4.046	6.035	7.496	8.875	10.09	11.12	11.88	12.36	12.39
20,000	.2170	2.723	4.602	6.672	8.267	9.845	11.19	12.18	12.92	13.45	13.52
22,000	.2115	2.826	4.975	7.182	8.997	10.64	12.09	13.31	14.22	14.69	14.77
24,000	.2066	3.020	5.427	7.621	9.640	11.56	13.16	14.52	15.41	16.02	16.13
26,000	.2020	3.217	5.828	8.249	10.49	12.45	14.20	15.65	16.75	17.37	17.57
28,000	.1970	3.415	6.288	8.883	11.25	13.36	15.26	16.78	18.03	18.82	19.09
Altitude, 150,000 ft											
10,000	0.2568	1.684	2.507	3.302	4.036	4.838	5.385	6.050	6.261	6.307	6.233
12,000	.2501	1.895	2.841	3.871	4.740	5.648	6.408	6.929	7.367	7.605	7.648
14,000	.2424	2.102	3.202	4.435	5.437	6.565	7.468	8.073	8.613	8.887	8.913
16,000	.2349	2.306	3.598	4.929	6.143	7.431	8.301	9.102	9.645	10.11	10.14
18,000	.2280	2.447	3.804	5.461	6.907	8.274	9.305	10.23	10.92	11.39	11.41
20,000	.2218	2.554	4.158	5.942	7.564	9.039	10.23	11.04	11.85	12.33	12.42
22,000	.2165	2.647	4.486	6.529	8.263	9.741	11.04	12.18	13.00	13.54	13.65
24,000	.2119	2.821	4.879	7.013	8.892	10.60	11.98	13.24	14.16	14.70	14.88
26,000	.2071	2.996	5.237	7.705	9.547	11.37	13.01	14.32	15.30	15.89	16.19
28,000	.2023	3.176	5.577	8.089	10.29	12.31	14.02	15.41	16.47	17.21	17.52
Altitude, 200,000 ft											
10,000	0.2533	1.722	2.603	3.357	3.562	4.993	5.778	6.223	6.538	6.783	6.650
12,000	.2470	1.987	2.948	4.178	5.031	5.662	6.708	7.379	7.834	8.115	7.970
14,000	.2397	2.222	3.404	4.746	5.796	6.887	7.673	8.403	9.006	9.358	9.335
16,000	.2323	2.224	3.808	5.199	6.511	7.758	8.763	9.616	10.24	10.64	10.69
18,000	.2259	2.433	3.938	5.724	7.275	8.578	9.766	10.75	11.46	11.96	12.04
20,000	.2201	2.627	4.604	6.575	7.915	9.421	10.78	11.62	12.40	12.93	12.99
22,000	.2151	2.803	4.795	6.895	8.607	10.07	11.49	12.72	13.60	14.13	14.31
24,000	.2110	2.968	5.169	7.265	9.632	11.01	12.54	13.78	14.80	15.42	15.62
26,000	.2065	3.120	5.490	7.866	9.956	11.90	13.55	14.90	15.95	16.64	16.95
28,000	.2015	3.273	5.984	8.413	10.65	12.72	14.53	15.99	17.35	18.01	18.35
Altitude, 250,000 ft											
10,000	0.2450	1.835	2.796	3.827	4.662	5.638	6.421	7.037	7.408	7.698	7.630
12,000	.2400	2.119	3.292	4.562	5.630	6.753	7.652	8.321	8.817	9.204	9.159
14,000	.2335	2.315	3.765	5.038	6.434	7.645	8.630	9.481	10.17	10.64	10.79
16,000	.2268	2.493	4.185	5.740	7.290	8.643	9.885	10.87	11.61	12.12	12.42
18,000	.2207	2.701	4.606	6.271	8.113	9.687	11.03	12.23	13.07	13.72	13.84
20,000	.2155	2.807	5.102	7.171	8.943	10.69	12.25	13.17	14.00	14.56	14.73
22,000	.2112	3.021	5.276	7.597	9.695	11.39	13.02	14.37	15.40	16.02	16.25
24,000	.2076	3.228	5.862	8.256	10.43	12.39	14.19	15.67	16.76	17.47	17.70
26,000	.2039	3.439	6.294	8.886	11.26	13.46	15.34	16.95	18.06	18.87	19.26
28,000	.1987	3.687	6.783	9.531	12.12	14.42	16.48	18.42	19.56	20.46	20.89
Altitude, 300,000 ft											
10,000	0.2453	-----	-----	-----	------	------	------	------	------	------	------
12,000	.2403	-----	-----	-----	------	------	------	------	------	------	------
14,000	.2337	2.333	3.722	5.046	6.449	7.700	8.707	9.536	10.18	10.70	10.82
16,000	.2272	2.496	4.199	5.821	7.366	8.685	9.855	10.85	11.63	12.24	12.48
18,000	.2215	2.630	4.622	6.567	8.182	9.722	11.02	12.16	13.26	13.86	13.95
20,000	.2166	2.811	4.715	7.120	9.033	10.74	12.24	13.12	14.03	14.56	14.80
22,000	.2128	3.019	5.453	7.673	9.763	11.41	13.03	14.41	15.42	16.07	16.23
24,000	.2096	3.235	5.948	8.320	10.40	12.36	14.11	15.56	16.76	17.44	17.77
26,000	.2060	3.443	6.301	8.944	11.27	13.43	15.50	16.88	18.14	18.95	19.33
28,000	.2009	3.661	6.657	9.430	12.05	14.50	16.46	18.11	19.50	20.41	20.84

TABLE III. - SKIN-FRICTION PARAMETER AT ZERO ANGLE OF ATTACK

Velocity, V, ft/sec	Skin-friction parameter, $C_{f,\alpha=0,\infty}(Re_\infty)^{1/2}$							
	Wall temperature, ^oR							
	1000	2000	2500	3000	1000	2000	2500	3000
	Altitude, 50,000 ft				Altitude, 100,000 ft			
10,000	0.5122	0.4928	0.4847	0.4716	0.5148	0.4954	0.4872	0.4798
12,000	.4870	.4726	.4662	.4559	.4896	.4751	.4688	.4630
14,000	.4649	.4541	.4491	.4409	.4676	.4567	.4519	.4473
16,000	.4459	.4373	.4336	.4270	.4486	.4404	.4366	.4331
18,000	.4292	.4226	.4195	.4143	.4324	.4260	.4229	.4202
20,000	.4147	.4095	.4070	.4027	.4184	.4133	.4109	.4086
22,000	.4019	.3977	.3957	.3922	.4063	.4024	.4005	.3986
24,000	.3907	.3873	.3856	.3825	.3958	.3927	.3912	.3895
26,000	.3802	.3771	.3756	.3729	.3859	.3825	.3810	.3795
28,000	.3702	.3675	.3663	.3639	.3758	.3728	.3716	.3704
	Altitude, 150,000 ft				Altitude, 200,000 ft			
10,000	0.5221	0.5028	0.4946	0.4871	0.5181	0.4987	0.4905	0.4833
12,000	.4969	.4825	.4763	.4704	.4928	.4783	.4720	.4664
14,000	.4750	.4642	.4595	.4549	.4711	.4603	.4556	.4511
16,000	.4562	.4479	.4442	.4408	.4522	.4444	.4408	.4374
18,000	.4402	.4339	.4310	.4283	.4369	.4307	.4279	.4254
20,000	.4265	.4217	.4194	.4173	.4238	.4190	.4169	.4149
22,000	.4149	.4112	.4094	.4077	.4127	.4093	.4076	.4061
24,000	.4051	.4022	.4009	.3992	.4037	.4012	.3982	.3982
26,000	.3954	.3921	.3906	.3890	.3945	.3912	.3897	.3881
28,000	.3851	.3822	.3809	.3795	.3841	.3813	.3800	.3787
	Altitude, 250,000 ft				Altitude, 300,000 ft			
10,000	0.5092	0.4901	0.4819	0.4744	0.5100	0.4906	0.4825	0.4751
12,000	.4841	.4696	.4635	.4577	.4847	.4701	.4641	.4585
14,000	.4625	.4518	.4471	.4428	.4629	.4525	.4481	.4438
16,000	.4441	.4363	.4327	.4295	.4449	.4373	.4340	.4308
18,000	.4289	.4231	.4207	.4180	.4303	.4248	.4222	.4198
20,000	.4165	.4122	.4103	.4084	.4185	.4145	.4126	.4109
22,000	.4064	.4032	.4018	.4005	.4091	.4063	.4050	.4039
24,000	.3983	.3961	.3950	.3937	.4020	.4001	.3985	.3979
26,000	.3900	.3867	.3851	.3836	.3941	.3909	.3892	.3876
28,000	.3796	.3769	.3756	.3742	.3838	.3810	.3796	.3782

TABLE IV. - HEAT-ENERGY PARAMETER AT ZERO ANGLE OF ATTACK

Velocity, V, ft/sec	Heat-energy parameter, $C_{q,\alpha=0}(Re_\infty)^{1/2}$							
	Wall temperature, ^oR							
	1000	2000	2500	3000	1000	2000	2500	3000
	Altitude, 50,000 ft				Altitude, 100,000 ft			
10,000	0.2478	0.2010	0.1796	0.1421	0.2501	0.2031	0.1814	0.1604
12,000	.2424	.2105	.1953	.1691	.2444	.2121	.1971	.1824
14,000	.2353	.2124	.2014	.1821	.2372	.2141	.2030	.1923
16,000	.2282	.2109	.2027	.1880	.2299	.2127	.2044	.1964
18,000	.2213	.2080	.2016	.1902	.2233	.2100	.2036	.1973
20,000	.2149	.2045	.1994	.1903	.2170	.2066	.2015	.1965
22,000	.2091	.2006	.1965	.1892	.2115	.2032	.1991	.1950
24,000	.2038	.1970	.1936	.1875	.2066	.1998	.1965	.1931
26,000	.1988	.1930	.1902	.1849	.2020	.1959	.1931	.1902
28,000	.1939	.1891	.1867	.1822	.1970	.1918	.1894	.1870
	Altitude, 150,000 ft				Altitude, 200,000 ft			
10,000	0.2568	0.2093	0.1872	0.1659	0.2533	0.2061	0.1843	0.1632
12,000	.2501	.2176	.2023	.1874	.2470	.2147	.1995	.1849
14,000	.2424	.2190	.2079	.1971	.2397	.2164	.2054	.1947
16,000	.2349	.2174	.2091	.2009	.2323	.2151	.2069	.1989
18,000	.2280	.2147	.2082	.2019	.2259	.2126	.2063	.2001
20,000	.2218	.2114	.2063	.2013	.2201	.2097	.2047	.1998
22,000	.2165	.2081	.2040	.2000	.2151	.2070	.2030	.1991
24,000	.2119	.2051	.2018	.1983	.2110	.2044	.2002	.1976
26,000	.2071	.2010	.1981	.1951	.2065	.2004	.1975	.1945
28,000	.2023	.1970	.1946	.1919	.2015	.1963	.1938	.1916
	Altitude, 250,000 ft				Altitude, 300,000 ft			
10,000	0.2450	0.1985	0.1770	0.1563	0.2453	0.1989	0.1774	0.1566
12,000	.2400	.2081	.1933	.1788	.2403	.2084	.1936	.1793
14,000	.2335	.2106	.1998	.1894	.2337	.2109	.2002	.1898
16,000	.2268	.2098	.2017	.1939	.2272	.2104	.2024	.1946
18,000	.2207	.2079	.2019	.1957	.2215	.2087	.2026	.1965
20,000	.2155	.2055	.2007	.1959	.2166	.2066	.2018	.1970
22,000	.2112	.2031	.1993	.1955	.2126	.2048	.2010	.1973
24,000	.2076	.2013	.1982	.1948	.2096	.2033	.2000	.1969
26,000	.2039	.1978	.1949	.1919	.2060	.1999	.1969	.1938
28,000	.1987	.1936	.1912	.1887	.2009	.1958	.1933	.1906

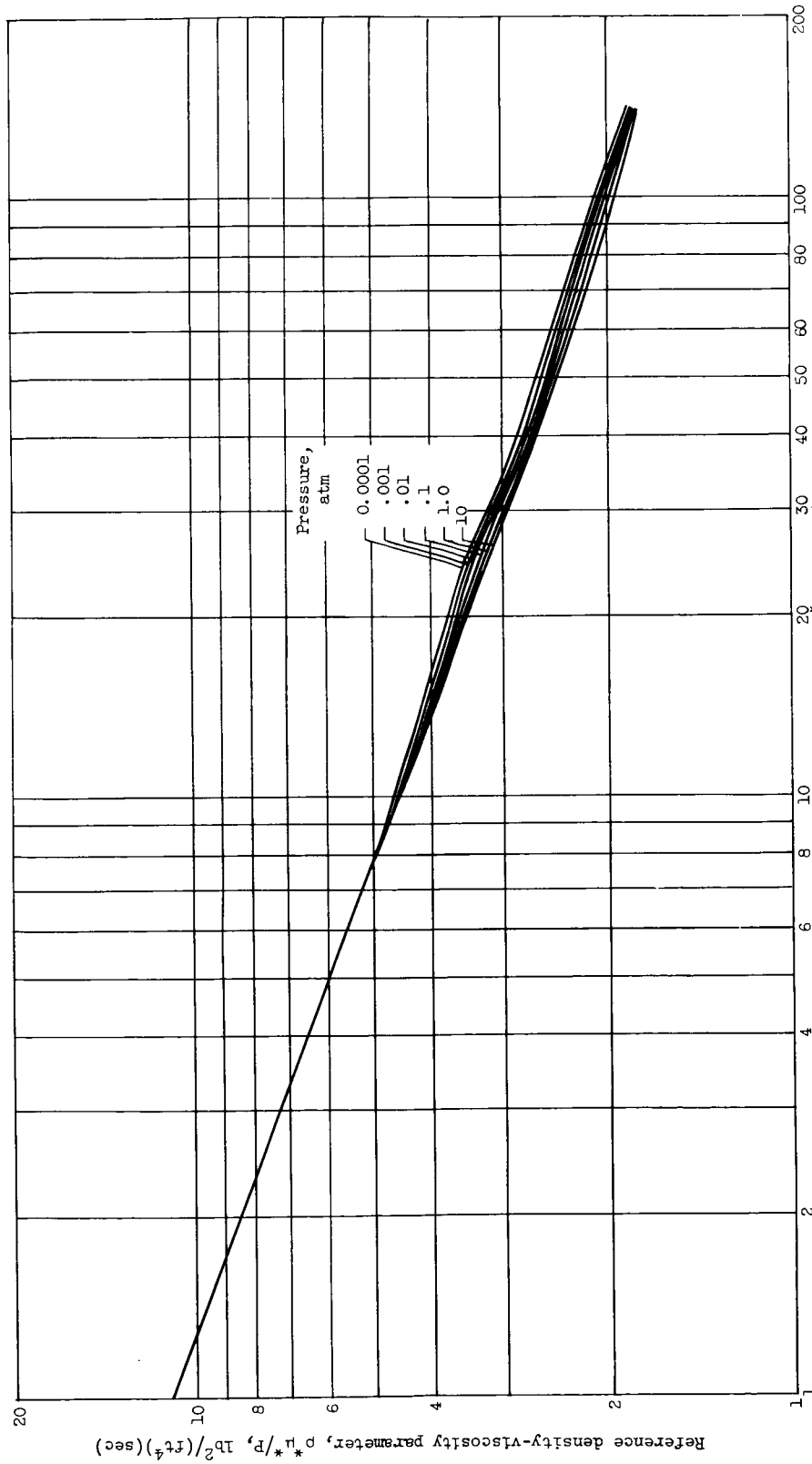

Figure 1. - Variation of product of reference density and viscosity $\rho^*\mu^*$ with reference enthalpy as a function of pressure (ref. 21).

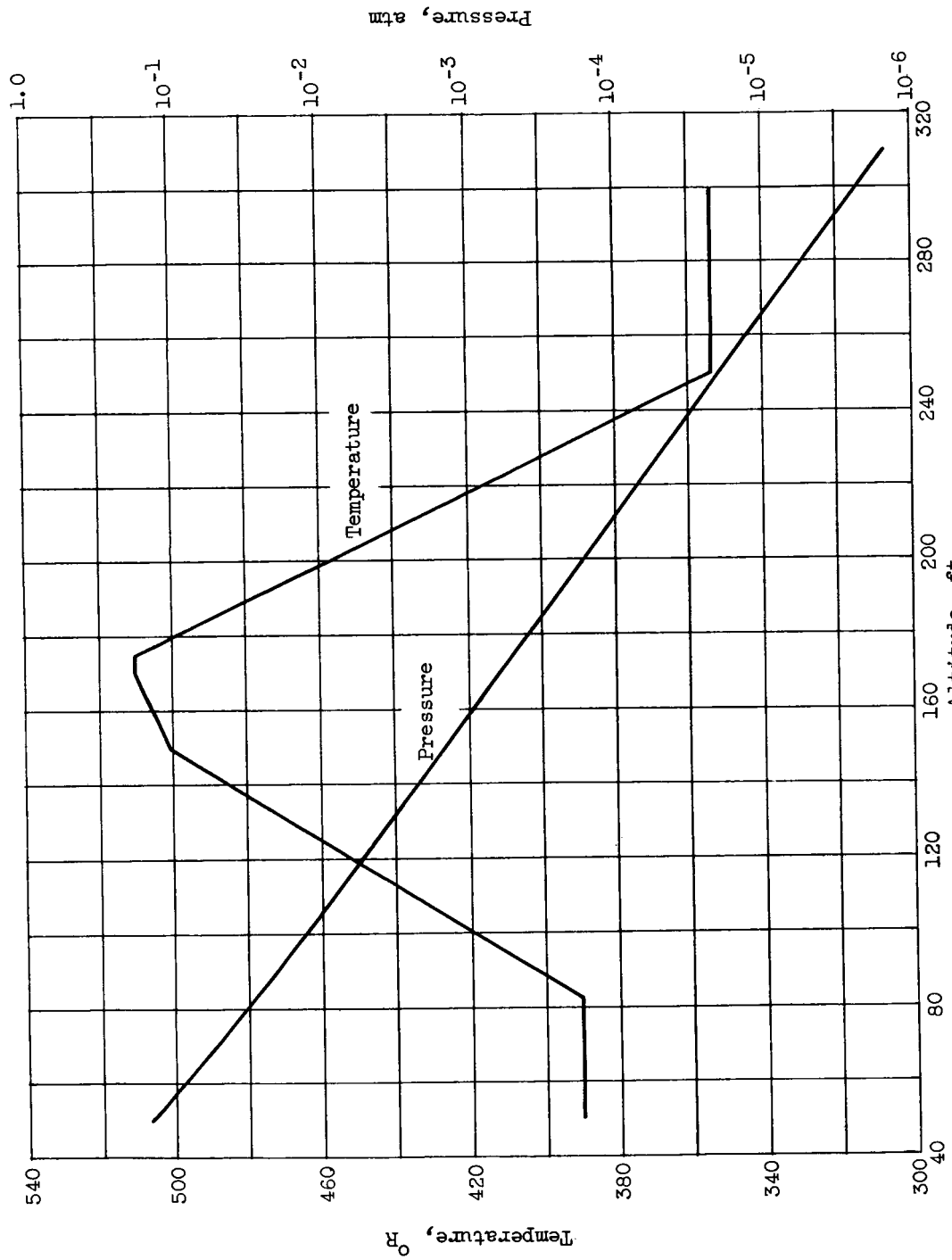

Figure 2. - Variation of atmospheric temperature and pressure with altitude from reference 18.

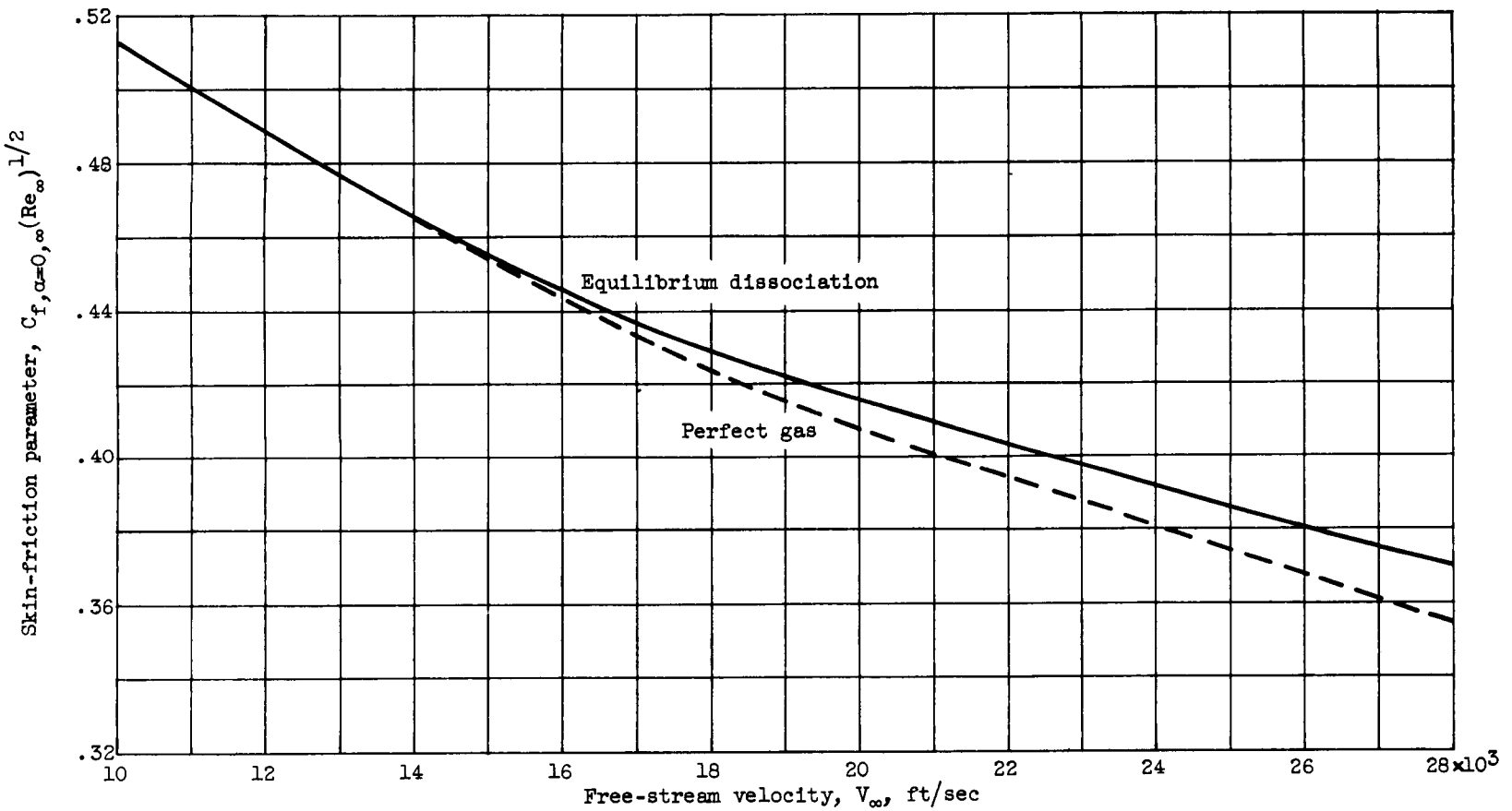

Figure 3. - Effect of equilibrium dissociation on laminar skin-friction parameter for a flat plate at zero angle of attack. Wall temperature, T_w, 1000° R; altitude, 50,000 feet; laminar boundary layer.

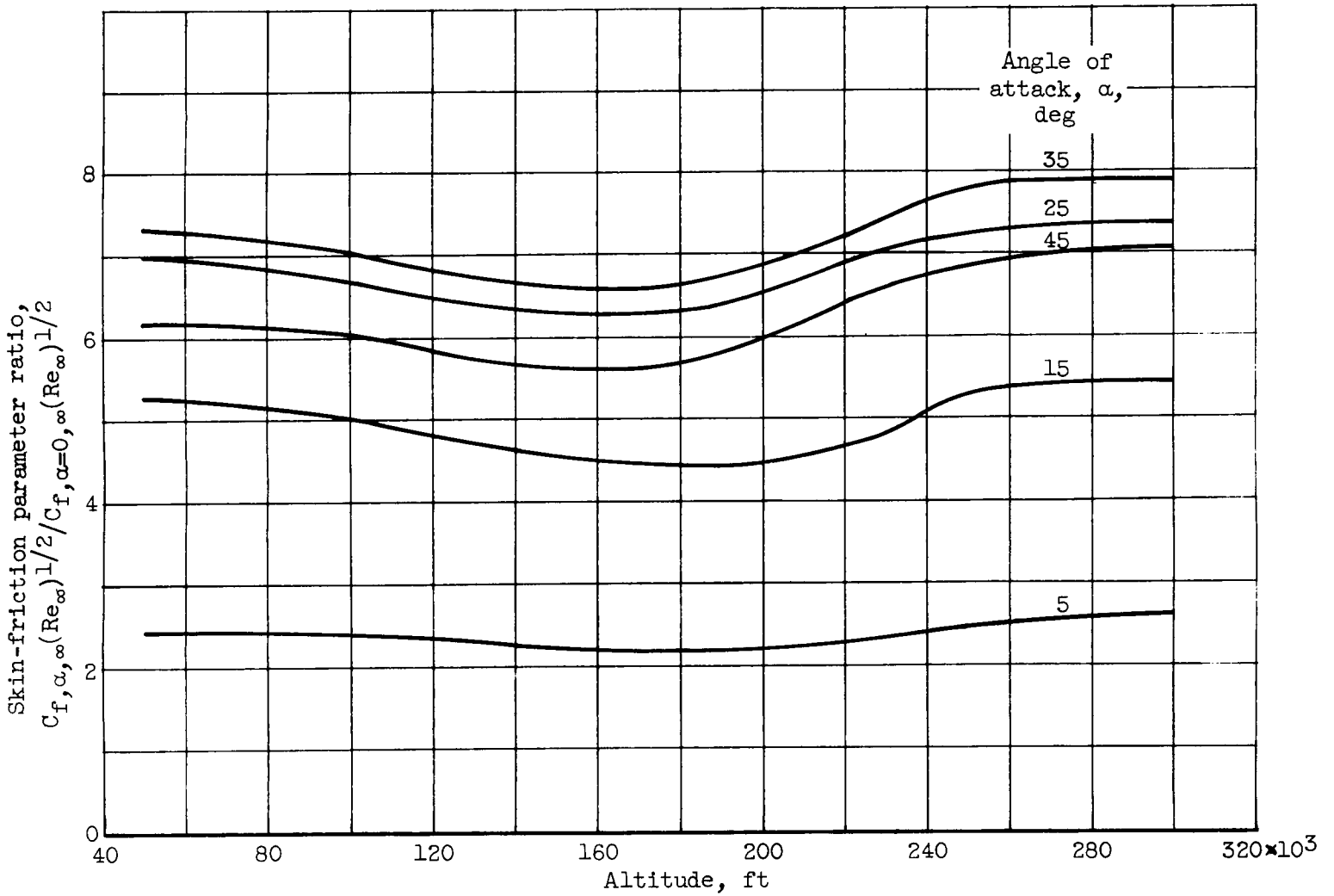

Figure 4. - Effect of altitude on skin-friction parameter ratio as a function of angle of attack. Wall temperature, T_w, 1000° R; velocity, 16,000 feet per second; laminar boundary layer.

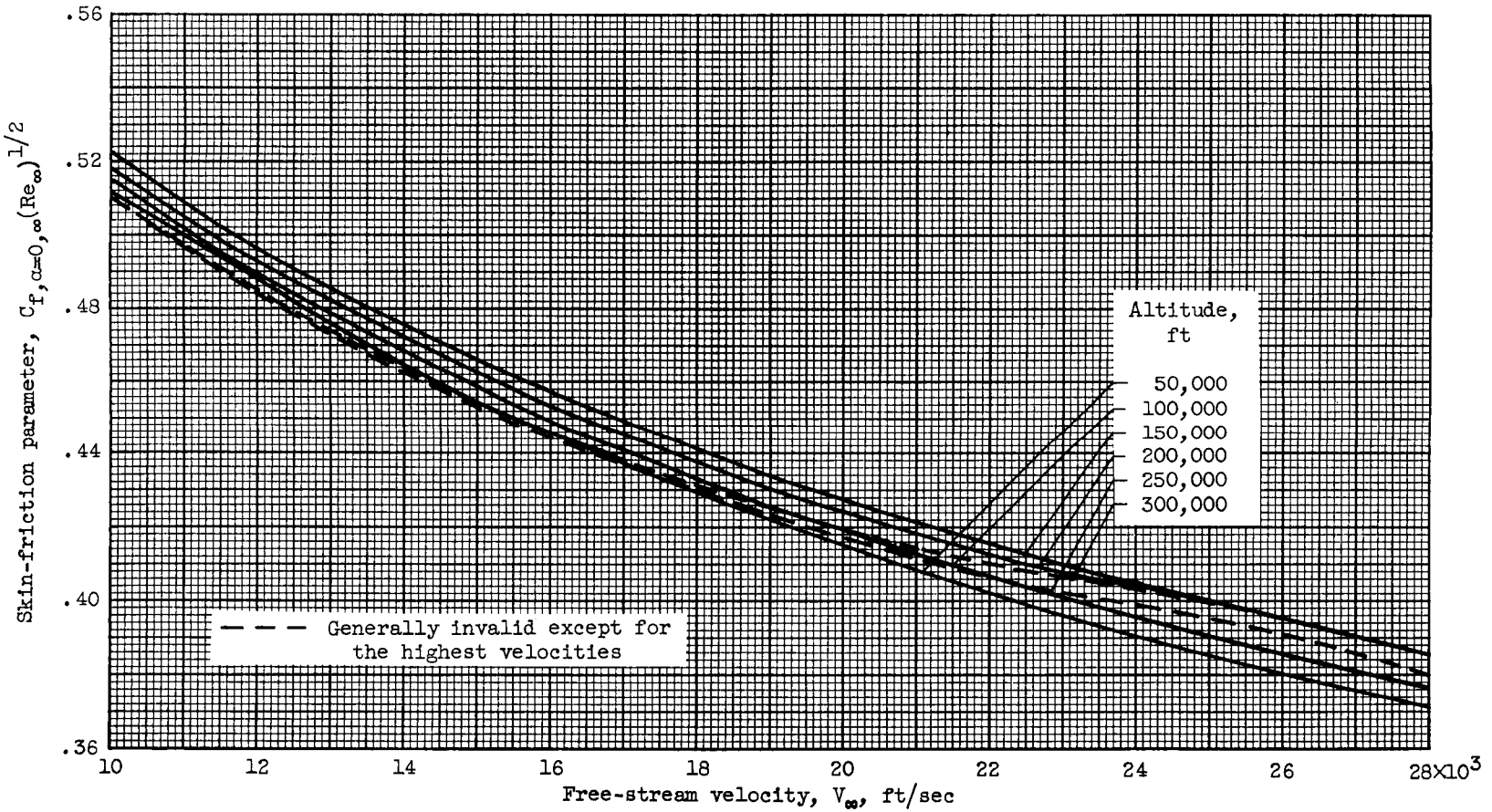

Figure 5. - Effect of velocity and altitude on skin-friction parameter for a flat plate at zero angle of attack. Wall temperature, T_w, 1000° R; laminar boundary layer.

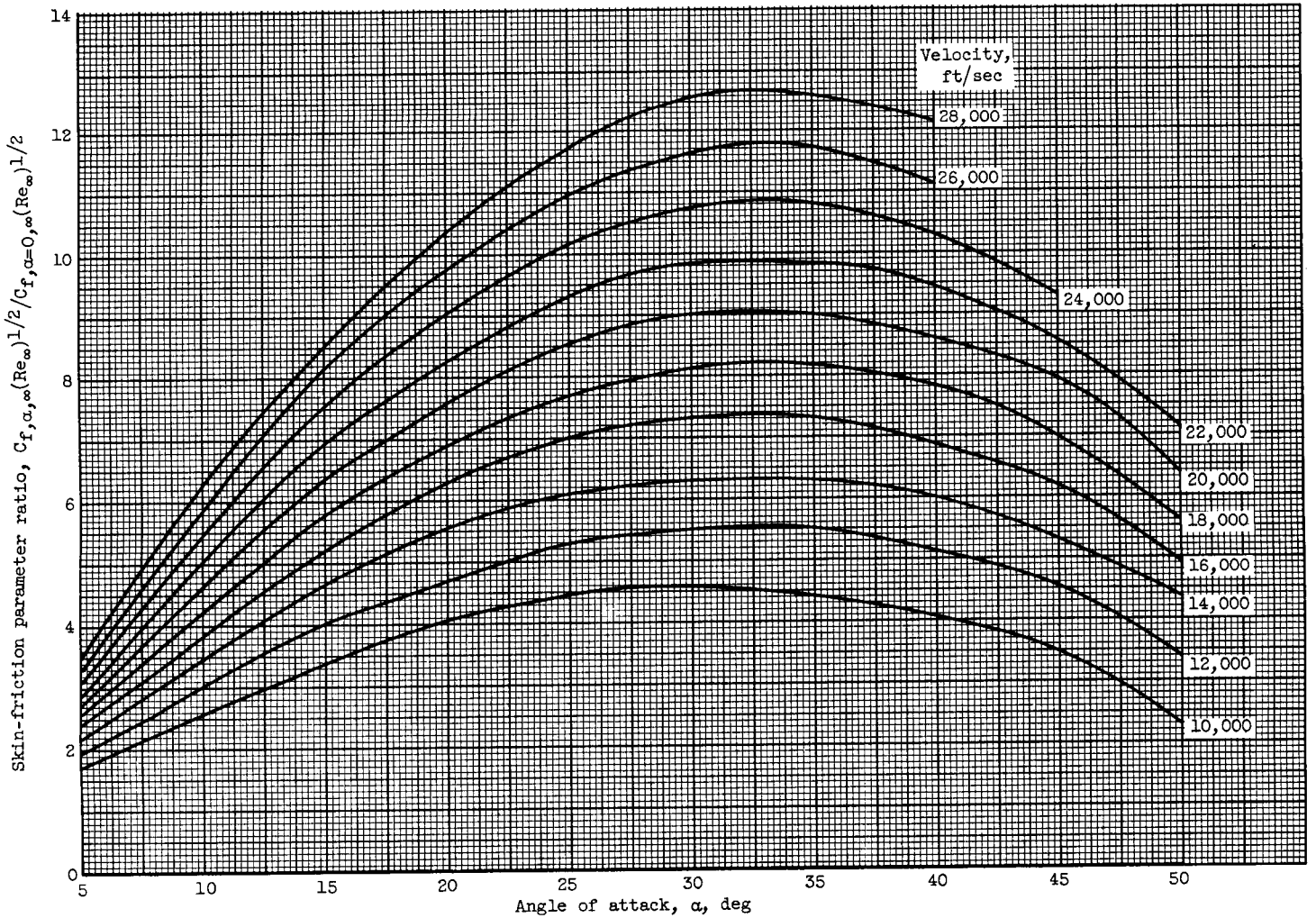

(a) Altitude, 50,000 feet.

Figure 6. - Effect of angle of attack on skin-friction parameter ratio as a function of velocity. Wall temperature, T_w, 1000° R; laminar boundary layer.

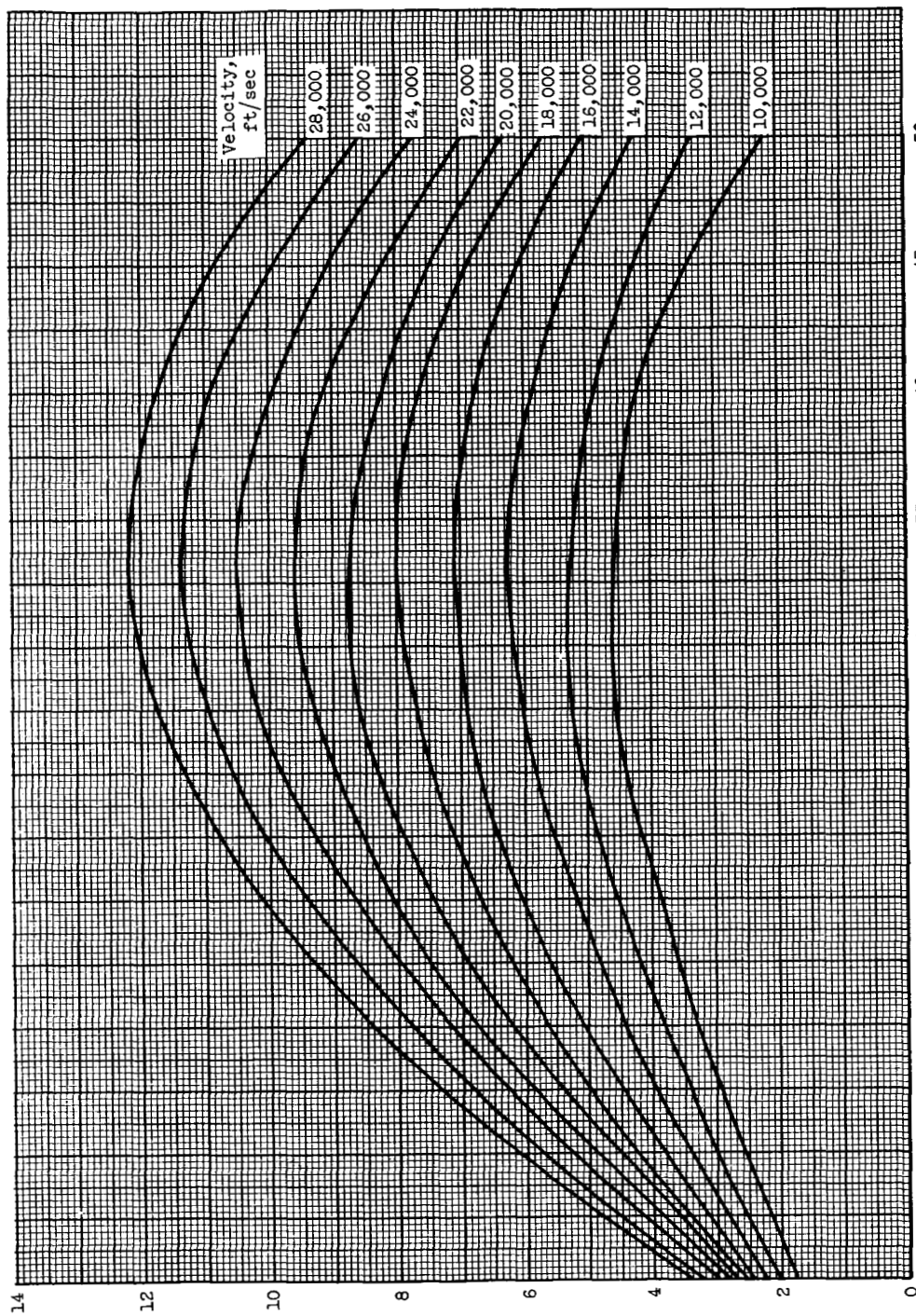

(b) Altitude, 100,000 feet.

Figure 6. - Continued. Effect of angle of attack on skin-friction parameter ratio as a function of velocity. Wall temperature, T_w, 1000° R; laminar boundary layer.

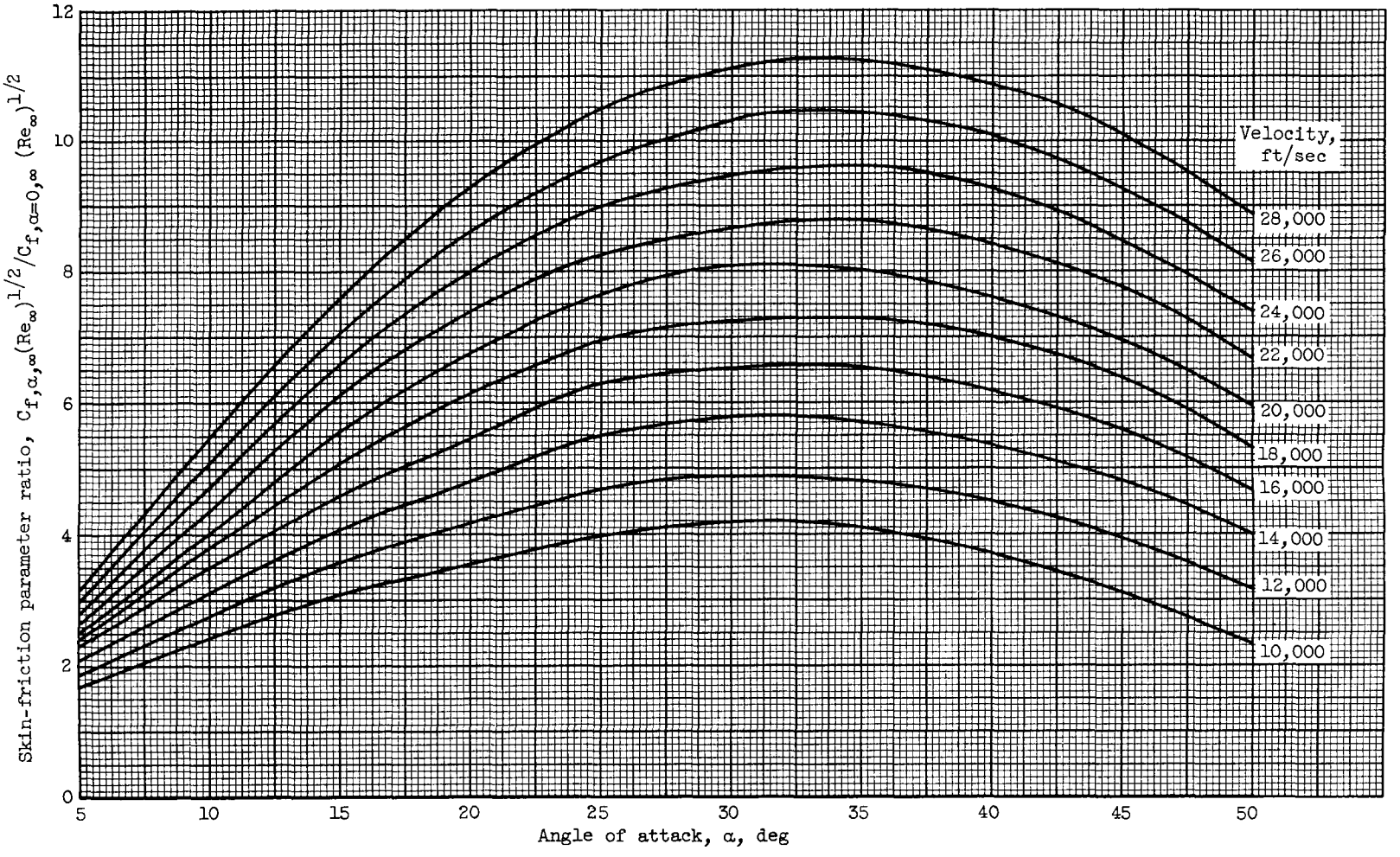

(c) Altitude, 150,000 feet.

Figure 6. - Continued. Effect of angle of attack on skin-friction parameter ratio as a function of velocity. Wall temperature, T_w, 1000° R; laminar boundary layer.

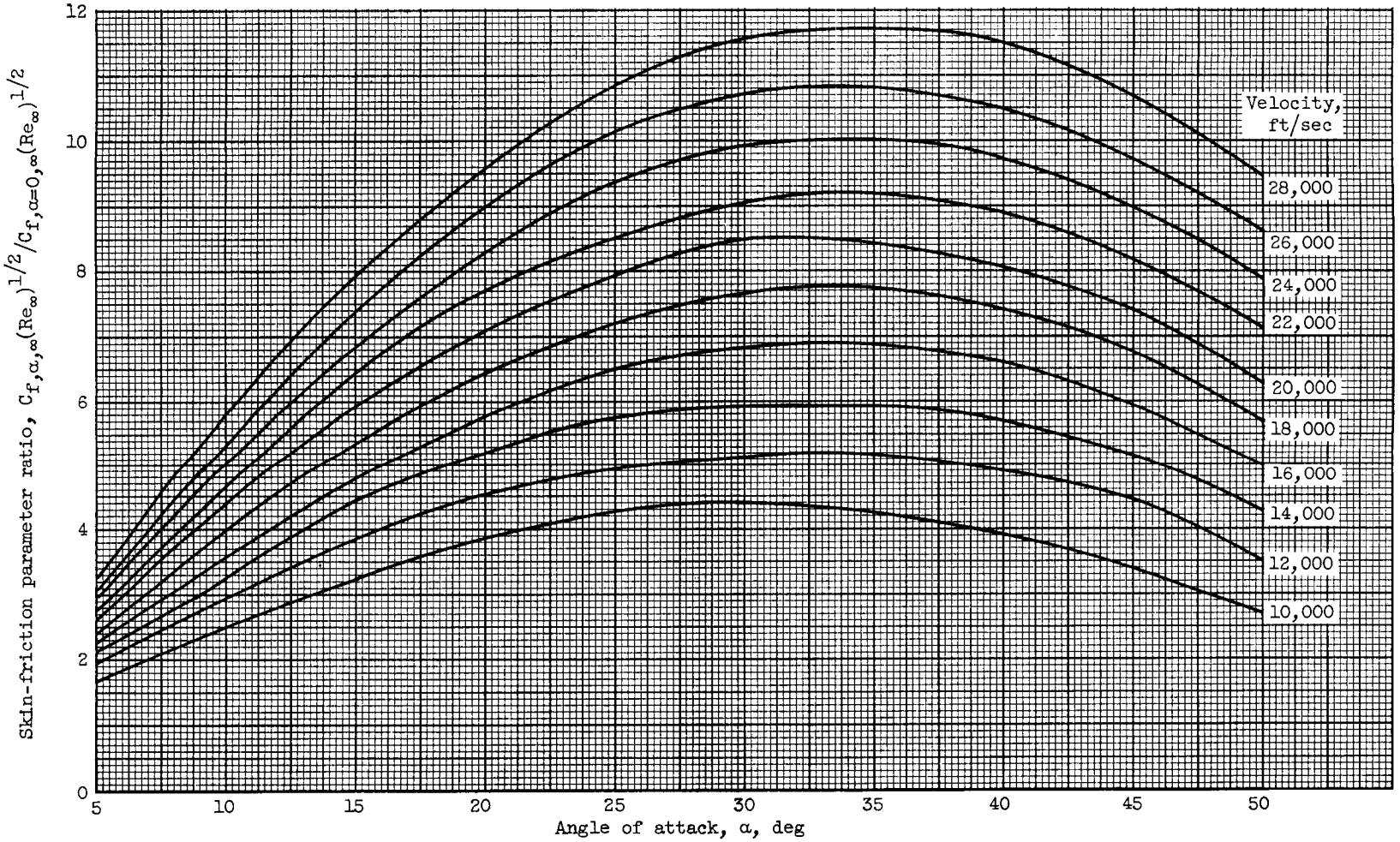

(d) Altitude, 200,000 feet.

Figure 6. - Continued. Effect of angle of attack on skin-friction parameter ratio as a function of velocity. Wall temperature, T_w, 1000° R; laminar boundary layer.

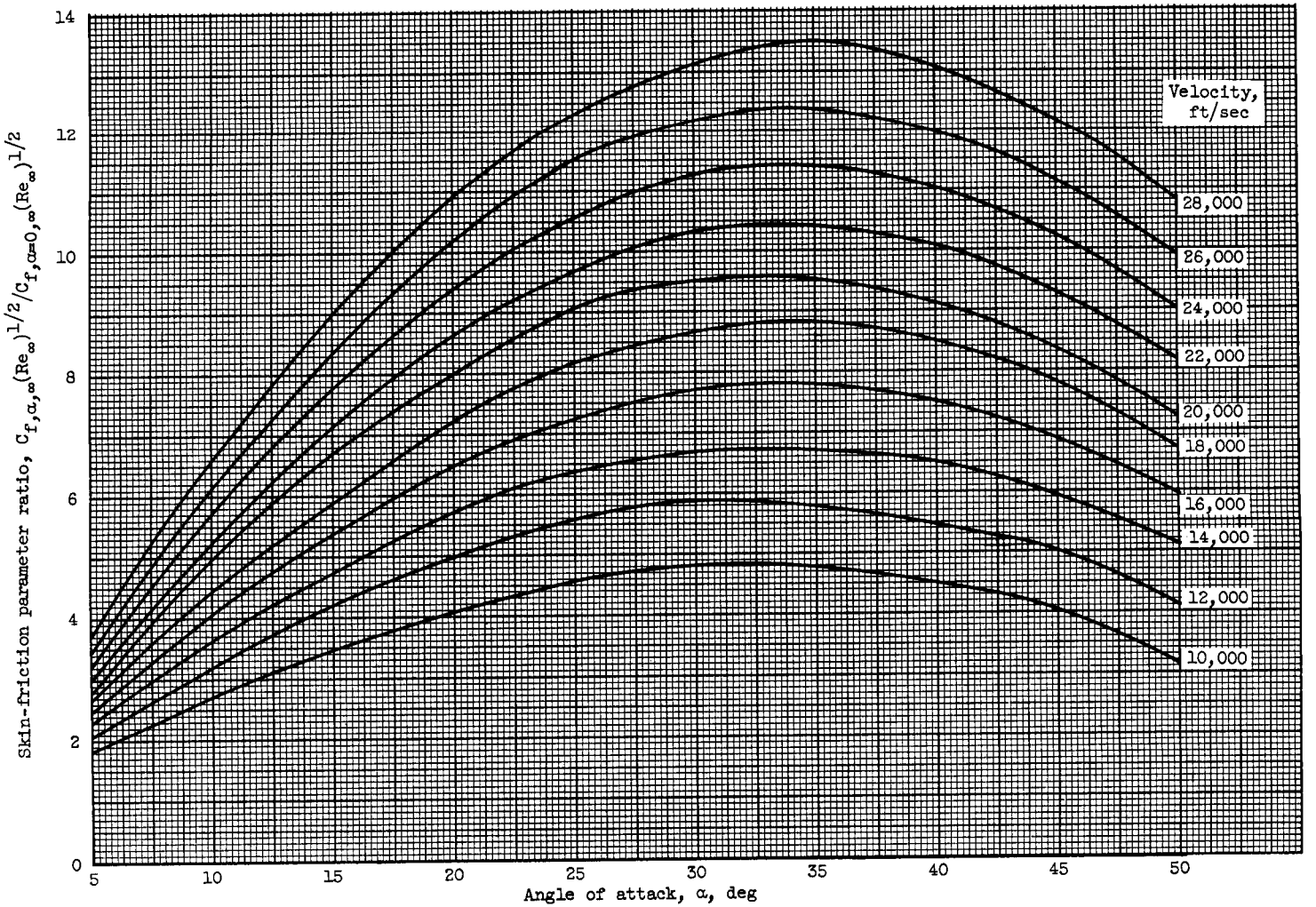

(e) Altitude, 250,000 feet.

Figure 6. - Continued. Effect of angle of attack on skin-friction parameter ratio as a function of velocity. Wall temperature, T_w, 1000° R; laminar boundary layer.

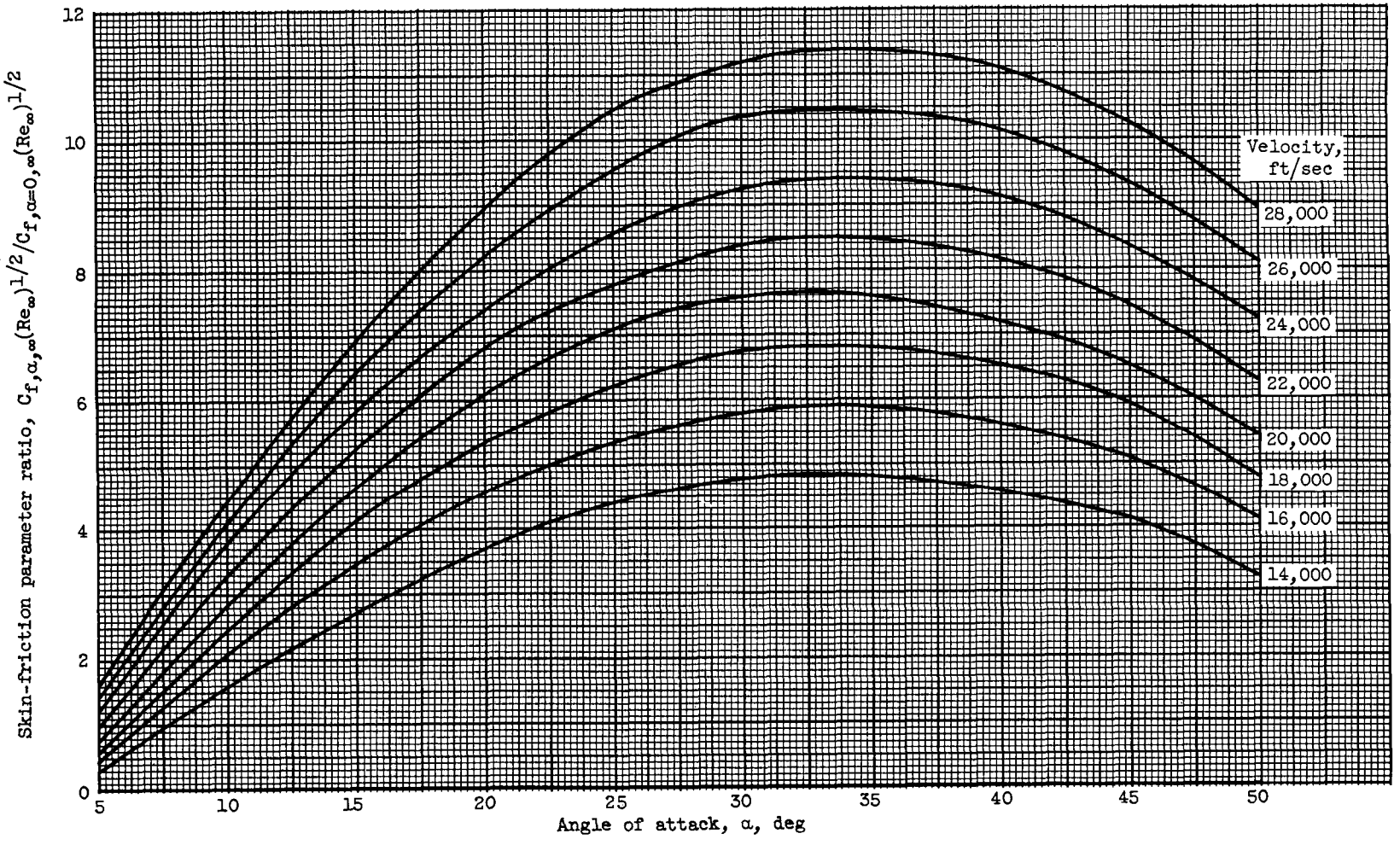

(f) Altitude, 300,000 feet.

Figure 6. - Concluded. Effect of angle of attack on skin-friction parameter ratio as a function of velocity. Wall temperature, T_w, 1000° F; laminar boundary layer.

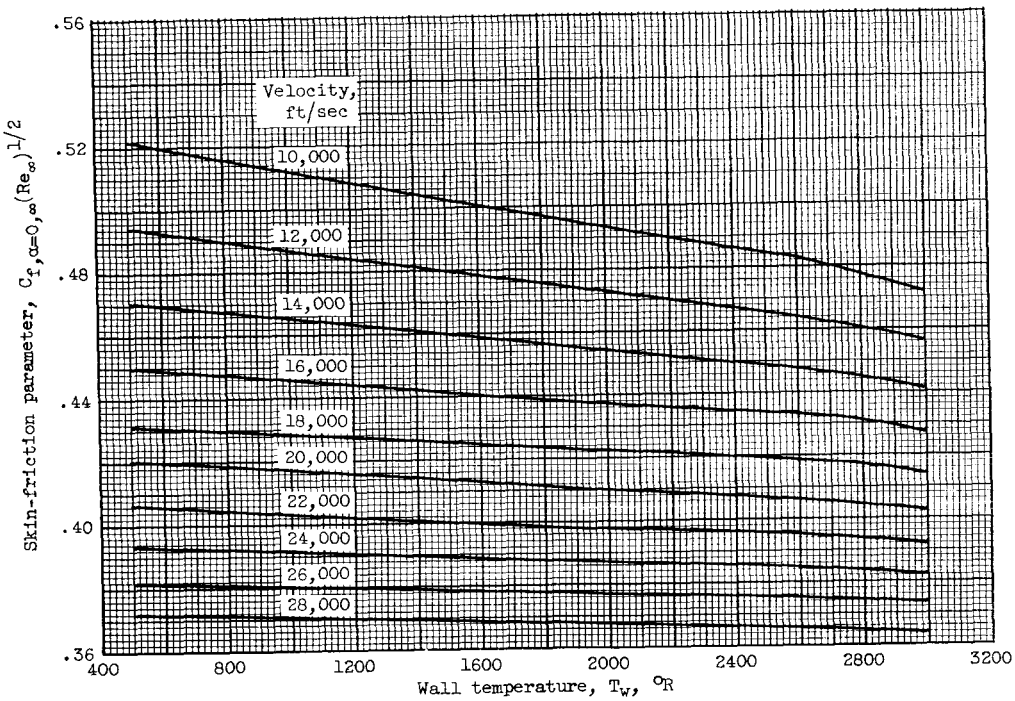

(a) Altitude, 50,000 feet.

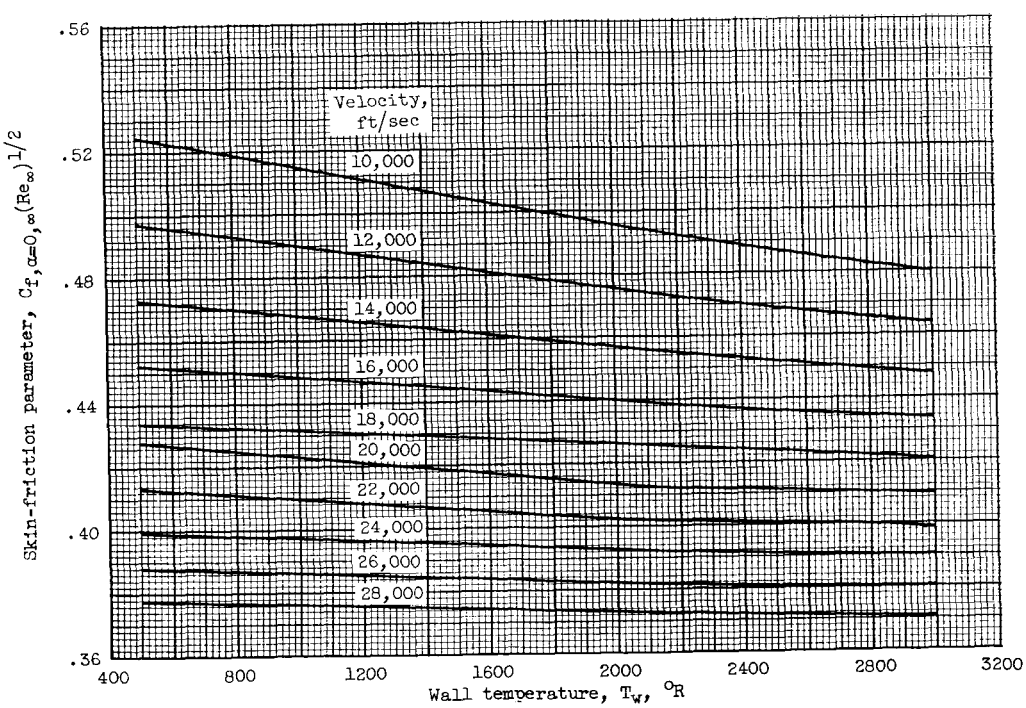

(b) Altitude, 100,000 feet.

Figure 7. - Effect of wall temperature on skin-friction parameter at zero angle of attack. Laminar boundary layer.

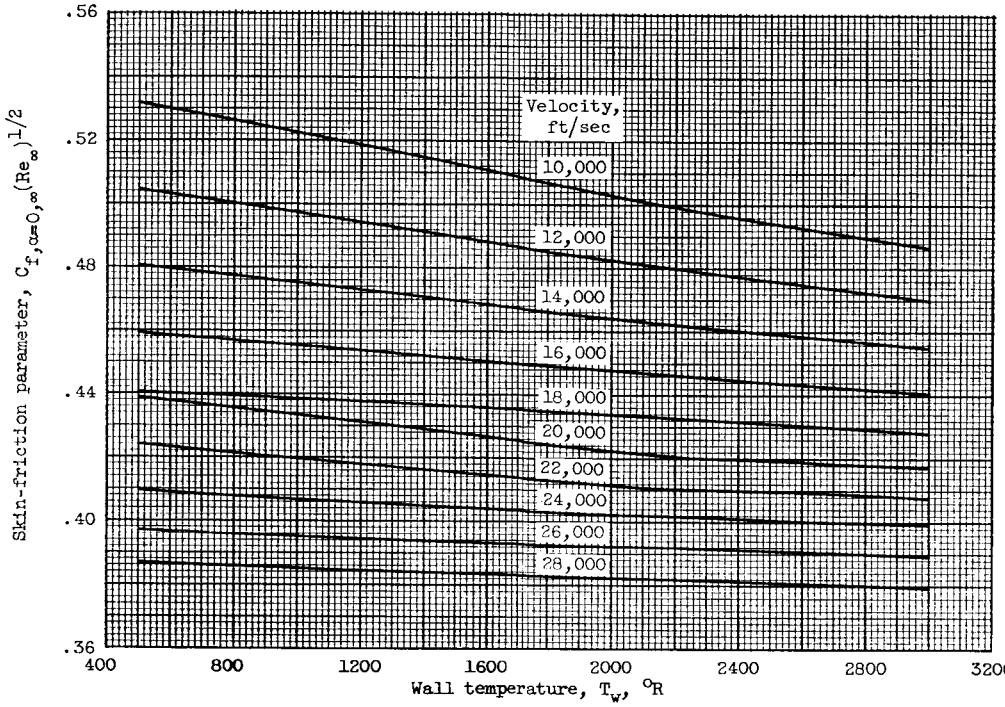

(c) Altitude, 150,000 feet.

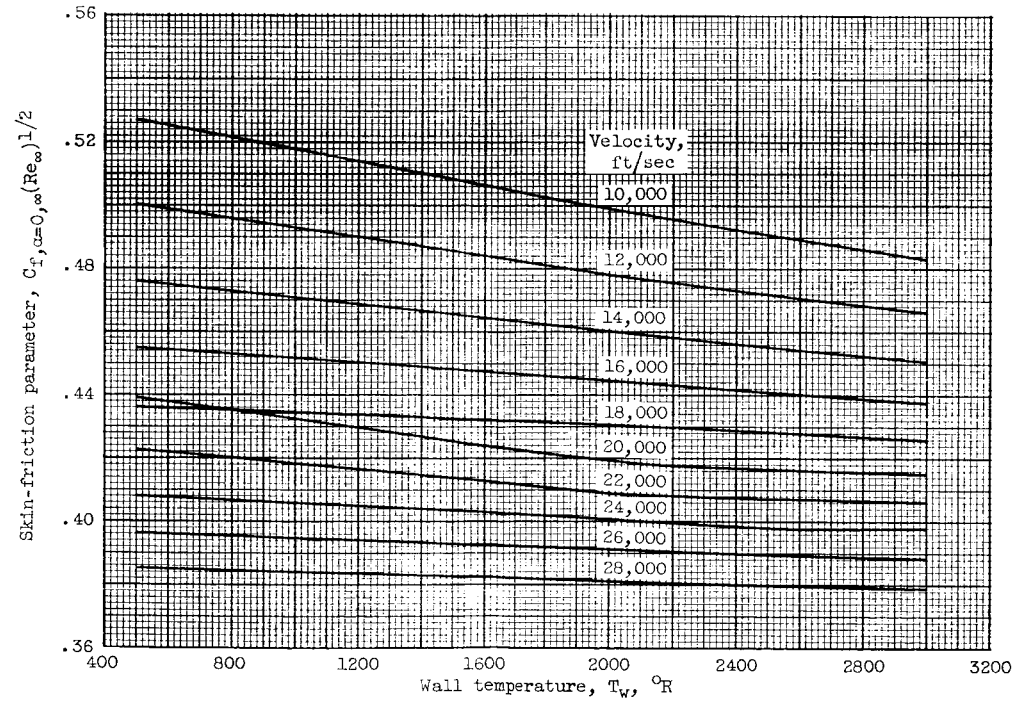

(d) Altitude, 200,000 feet.

Figure 7. - Continued. Effect of wall temperature on skin-friction parameter at zero angle of attack. Laminar boundary layer.

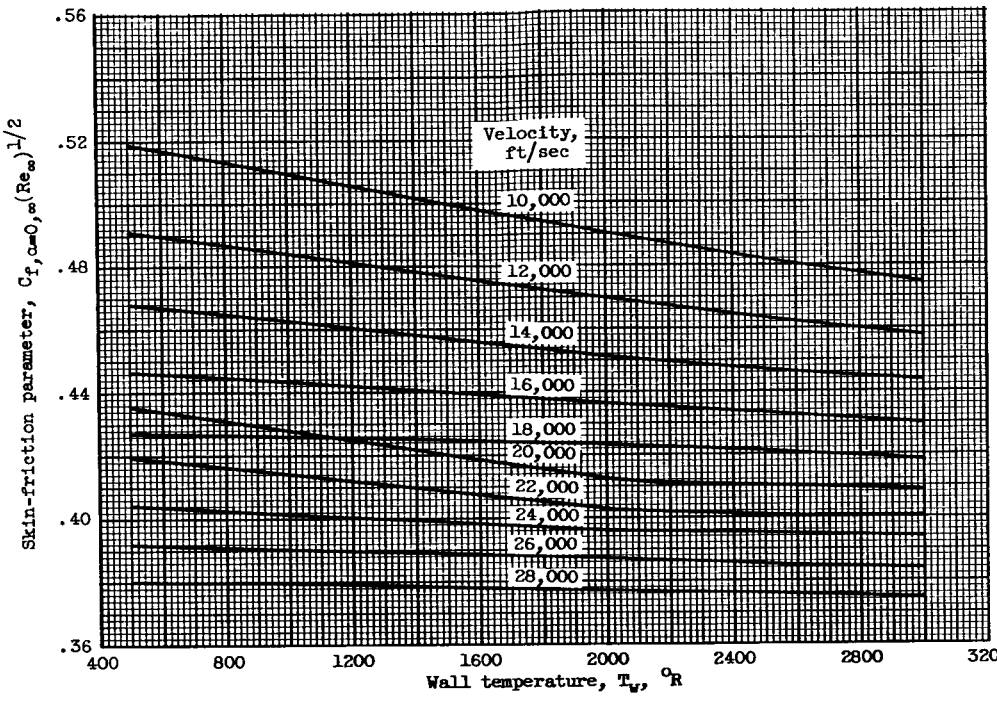

(e) Altitude, 250,000 feet.

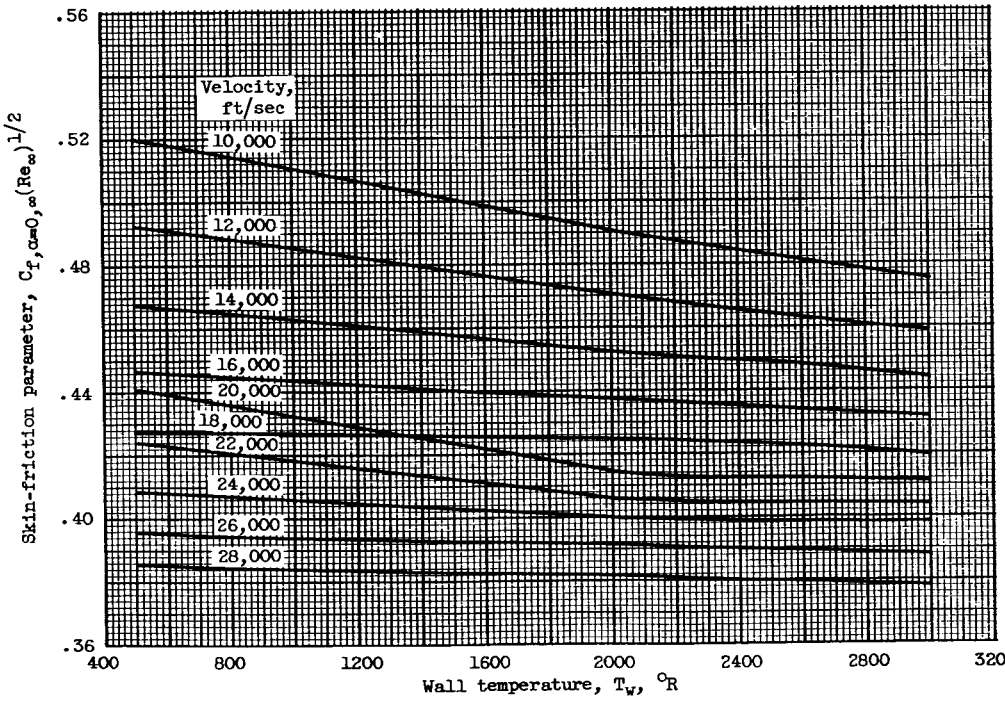

(f) Altitude, 300,000 feet.

Figure 7. - Concluded. Effect of wall temperature on skin-friction parameter at zero angle of attack. Laminar boundary layer.

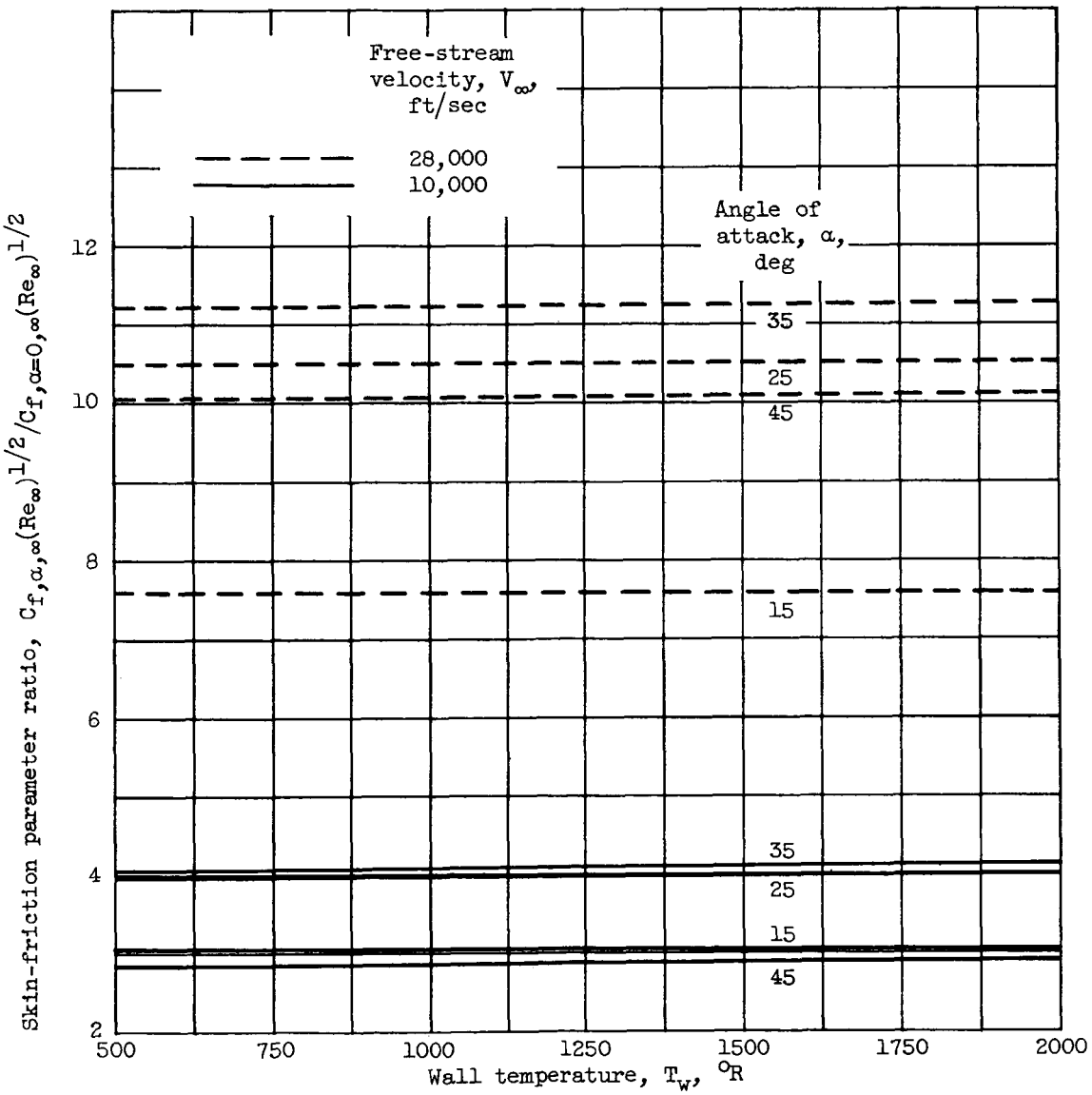

Figure 8. - Effect of wall temperature on laminar skin-friction parameter ratio as a function of angle of attack. Altitude, 150,000 feet; laminar boundary layer.

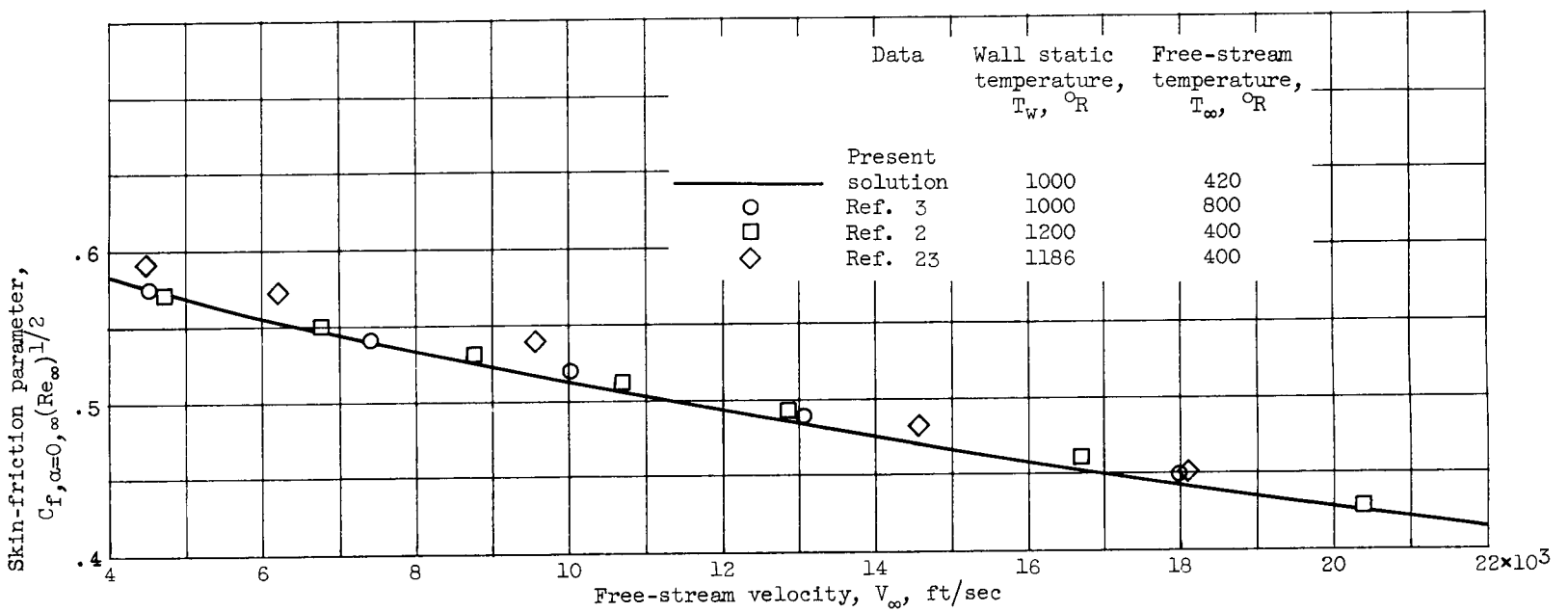

Figure 9. - Comparison of present solution with various solutions for laminar skin-friction parameter. Laminar boundary layer.

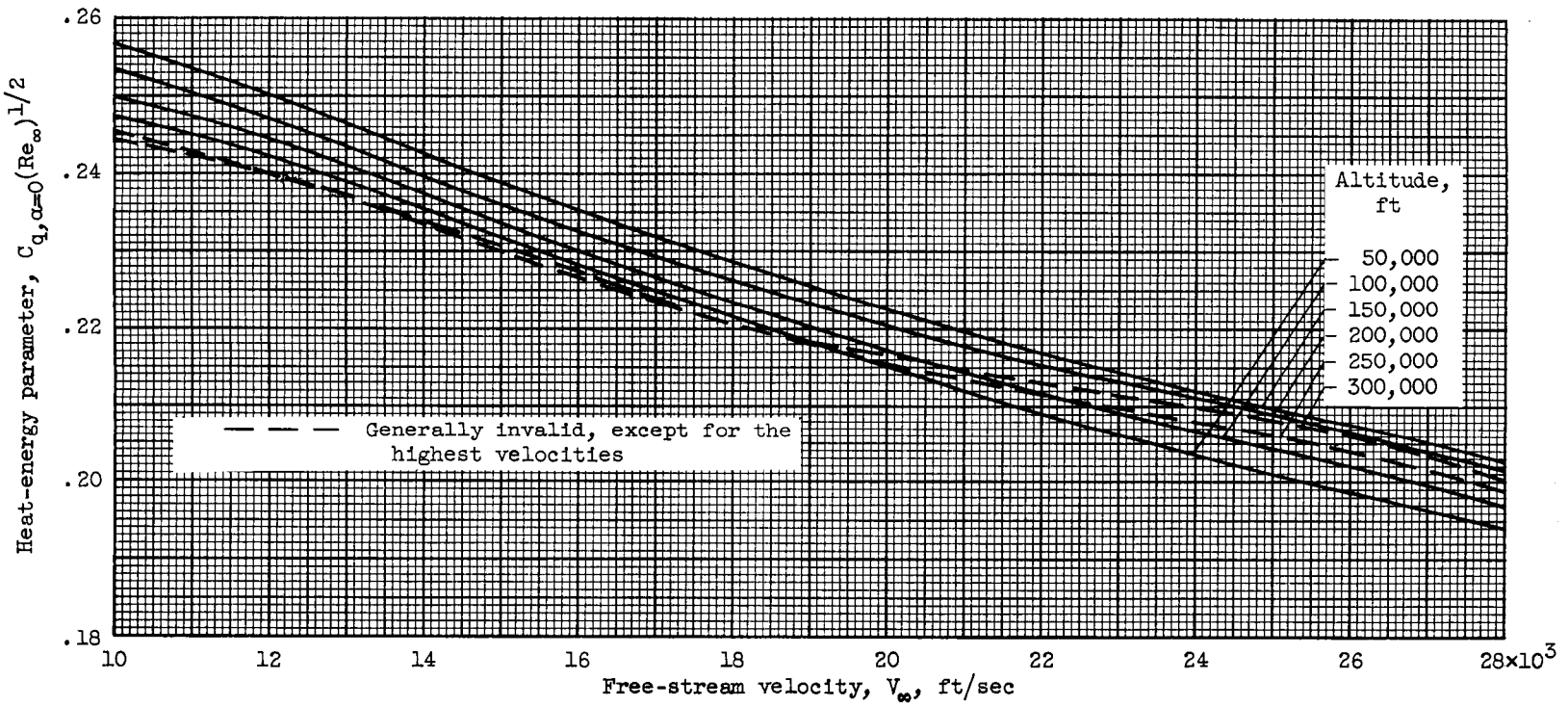

Figure 10. - Effect of velocity and altitude on heat-energy parameter for a flat plate at zero angle of attack. Wall static temperature, 1000° R; laminar boundary layer.

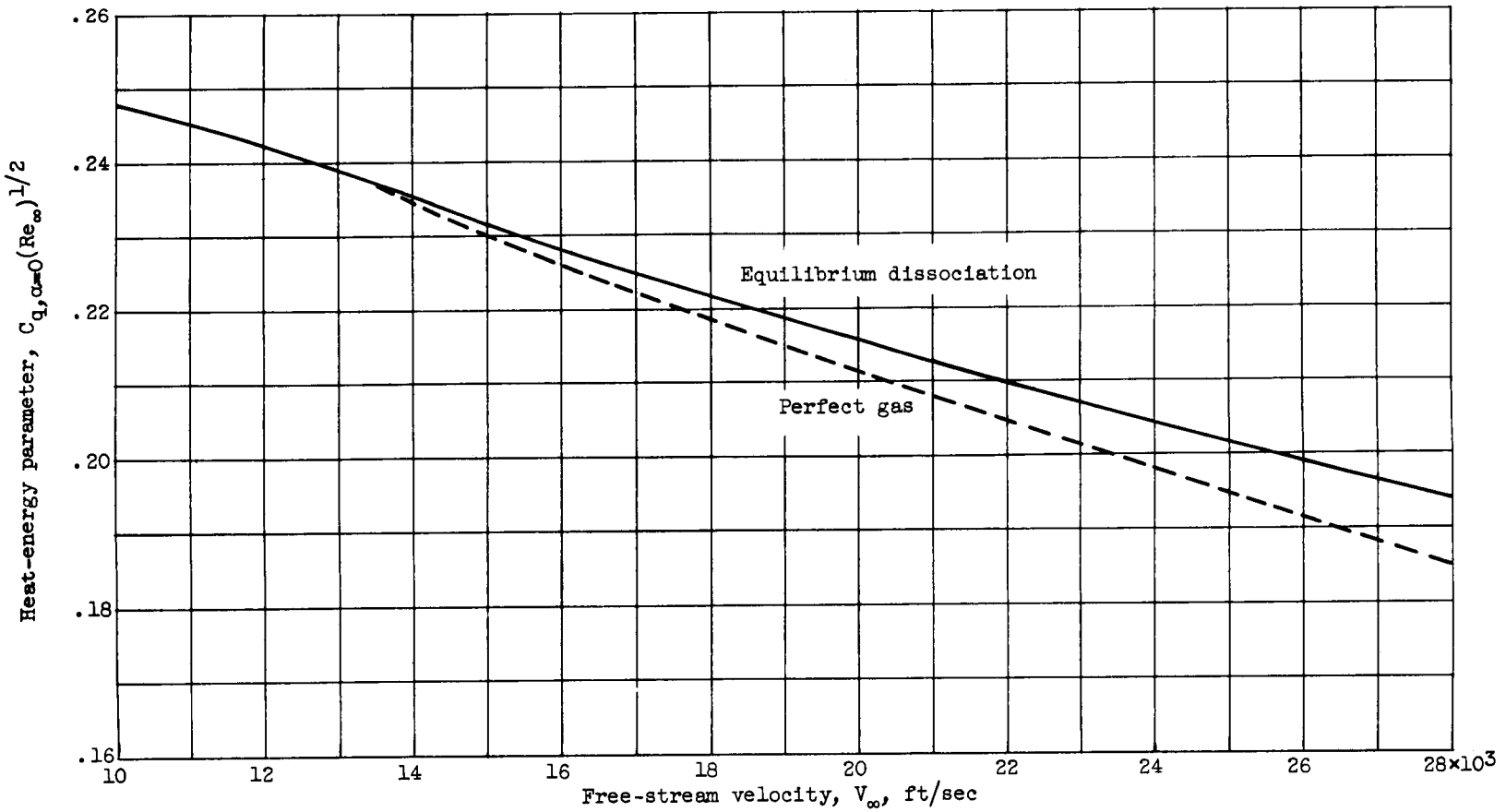

Figure 11. - Effect of equilibrium dissociation on laminar heat-energy parameter at zero angle of attack. Wall static temperature, 1000° R; altitude, 50,000 feet.

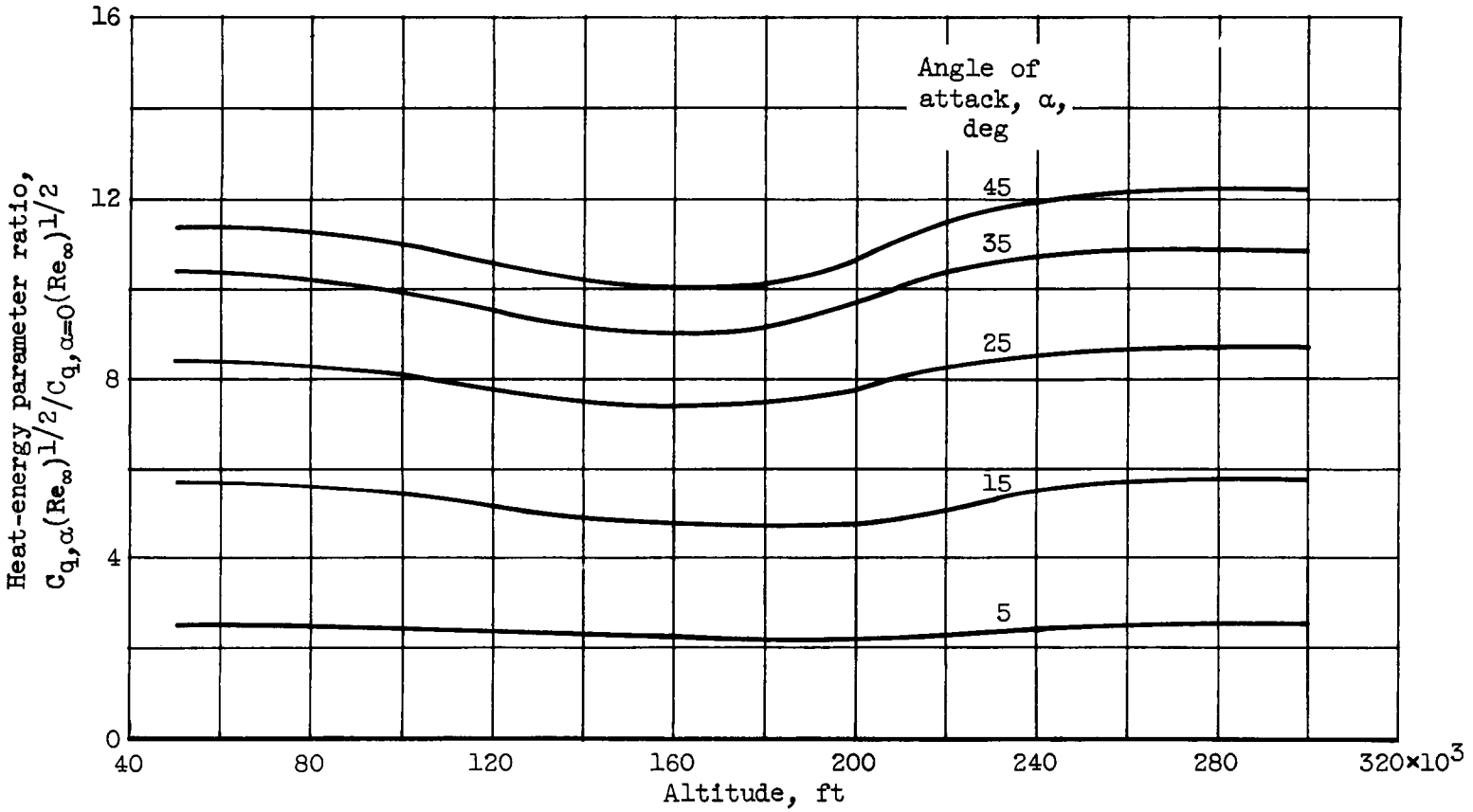

Figure 12. - Effect of altitude on heat-energy parameter ratio as a function of angle of attack. Wall temperature, T_w, 1000° R; velocity, 16,000 feet per second; laminar boundary layer.

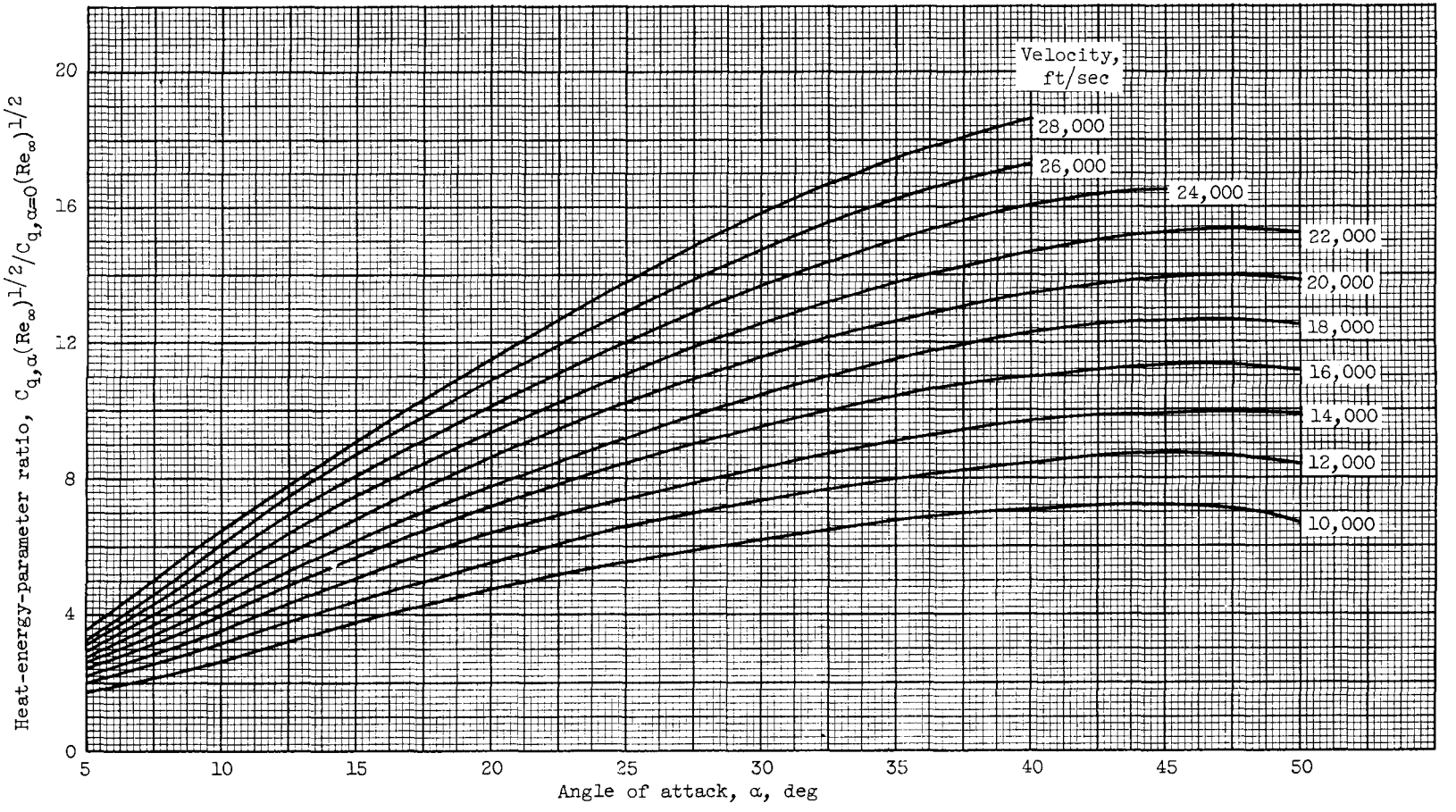

(a) Altitude, 50,000 feet.

Figure 13. - Effect of angle of attack on heat-energy parameter ratio as a function of velocity. Wall temperature, T_w, 1000° R; laminar boundary layer.

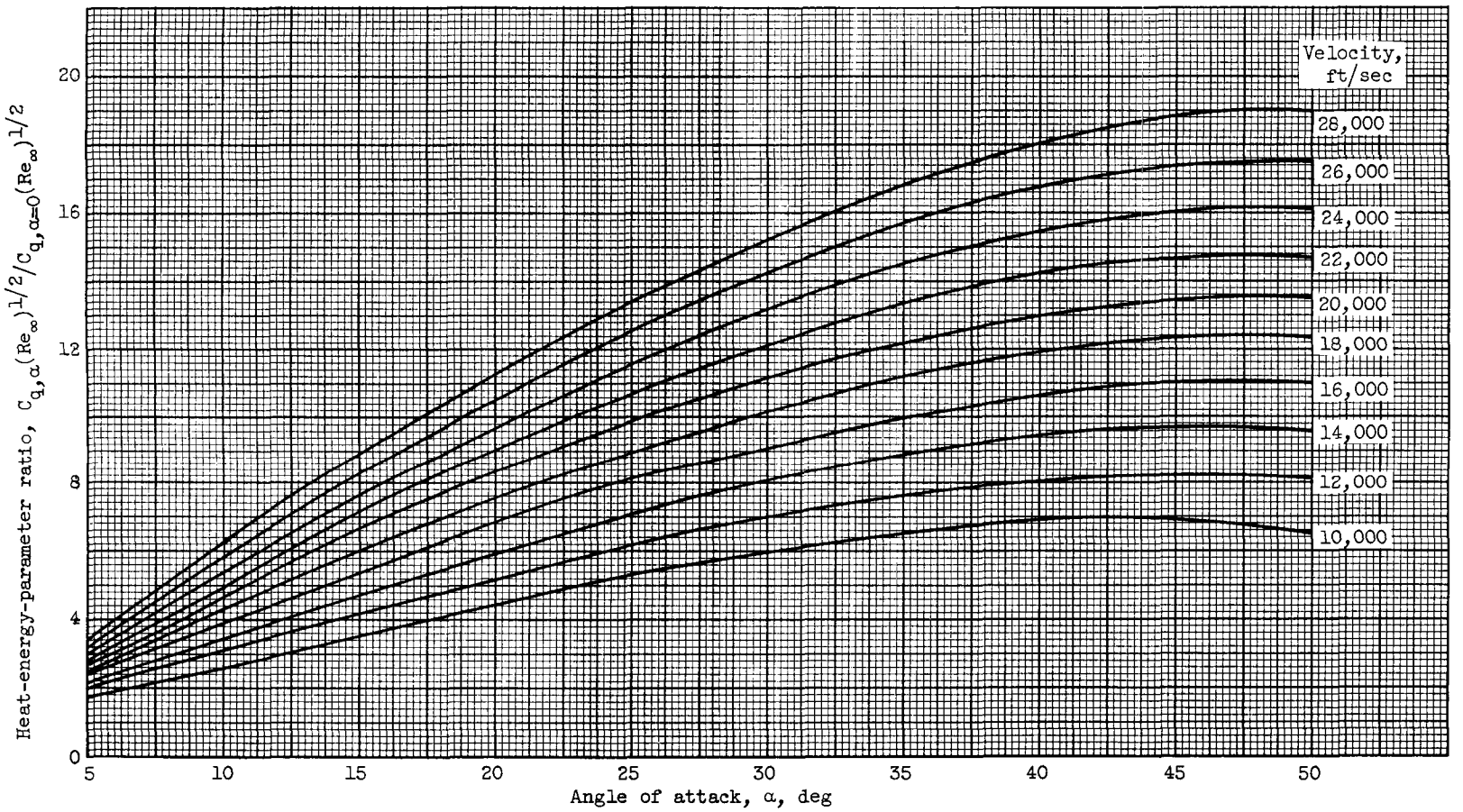

(b) Altitude, 100,000 feet.

Figure 13. - Continued. Effect of angle of attack on heat-energy parameter ratio as a function of velocity. Wall temperature, T_w, 1000° R; laminar boundary layer.

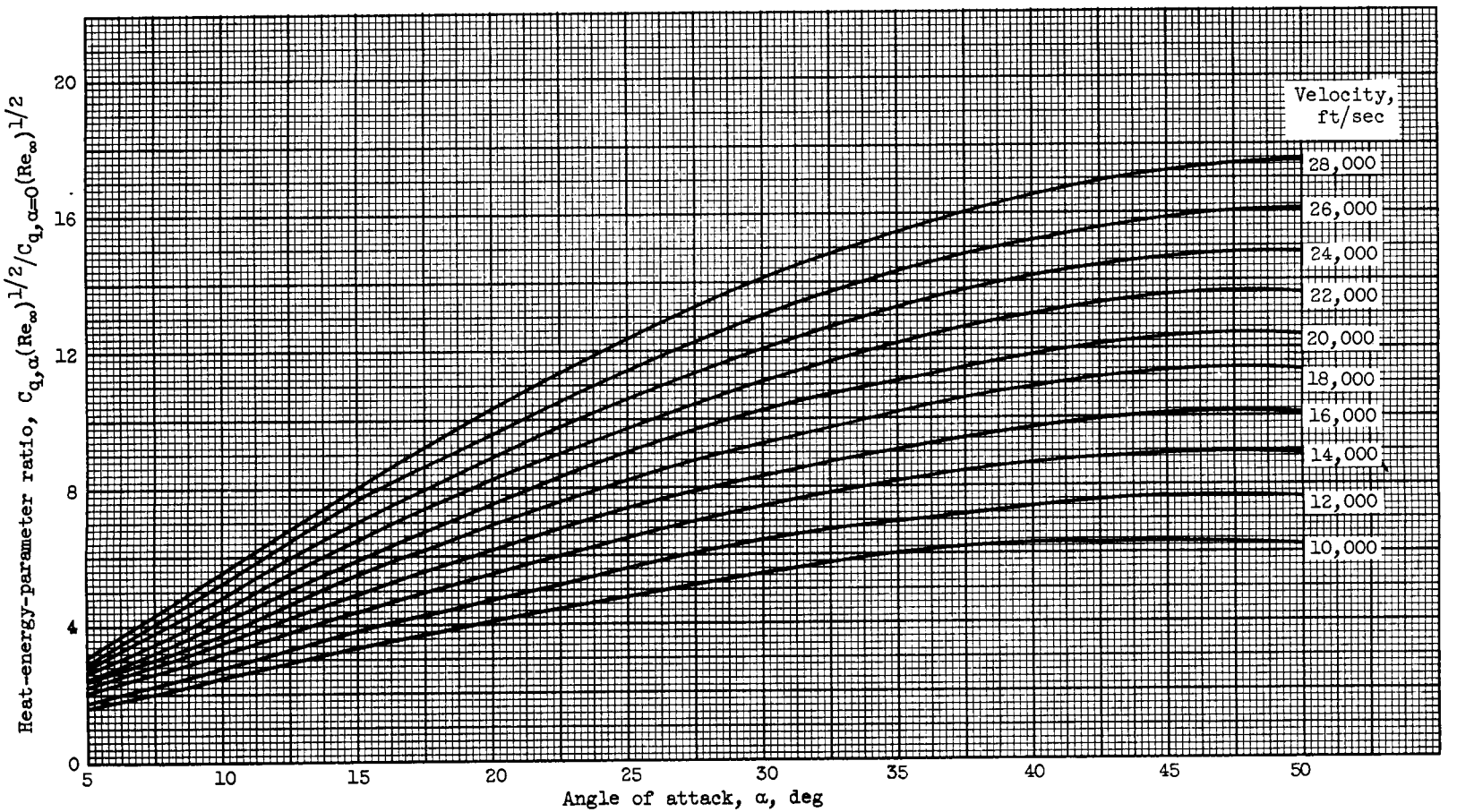

(c) Altitude, 150,000 feet.

Figure 13. - Continued. Effect of angle of attack on heat-energy-parameter ratio as a function of velocity. Wall temperature, T_w, 1000° R; laminar boundary layer.

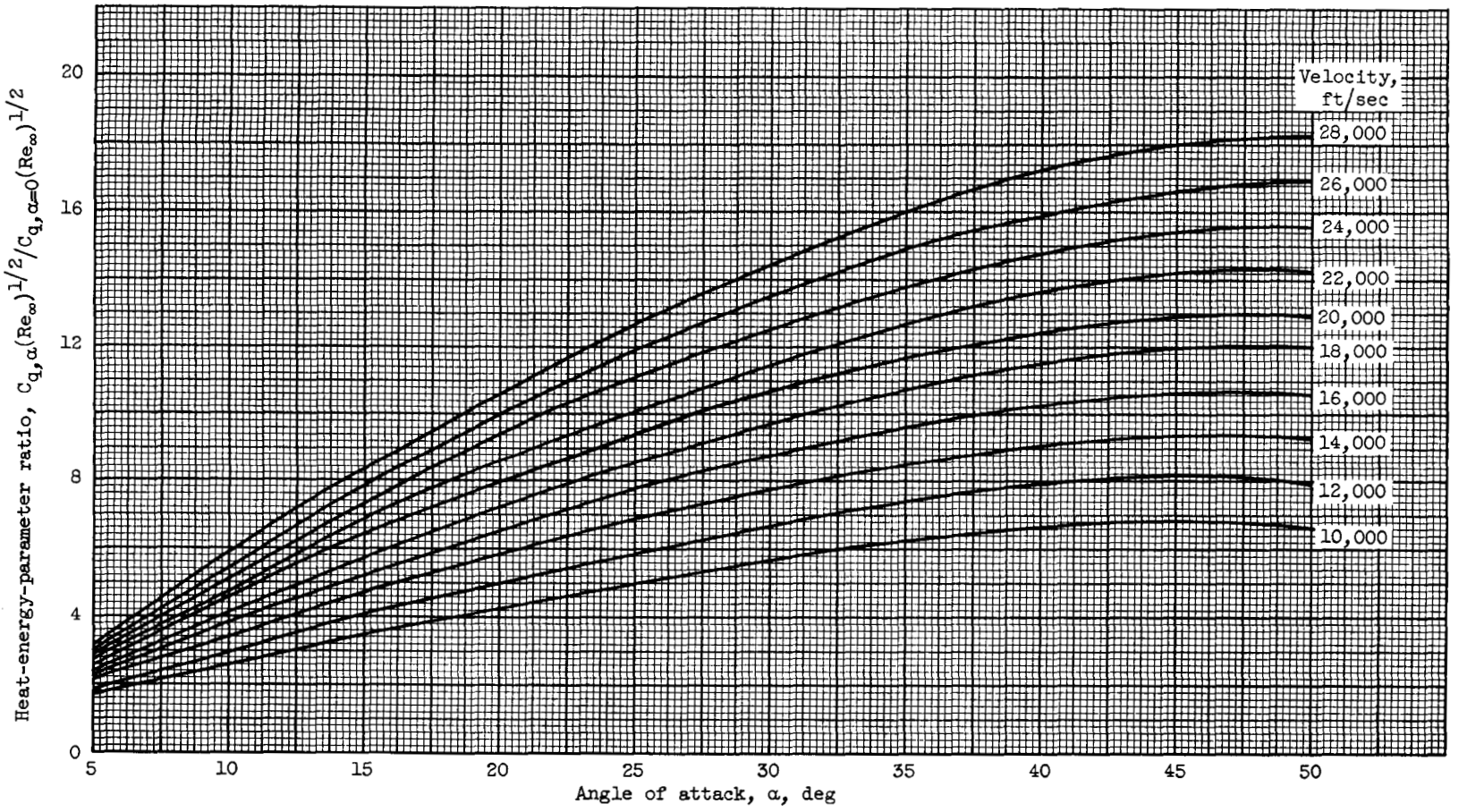

(d) Altitude, 200,000 feet.

Figure 13. - Continued. Effect of angle of attack on heat-energy-parameter ratio as a function of velocity. Wall temperature, T_w, 1000° R; laminar boundary layer.

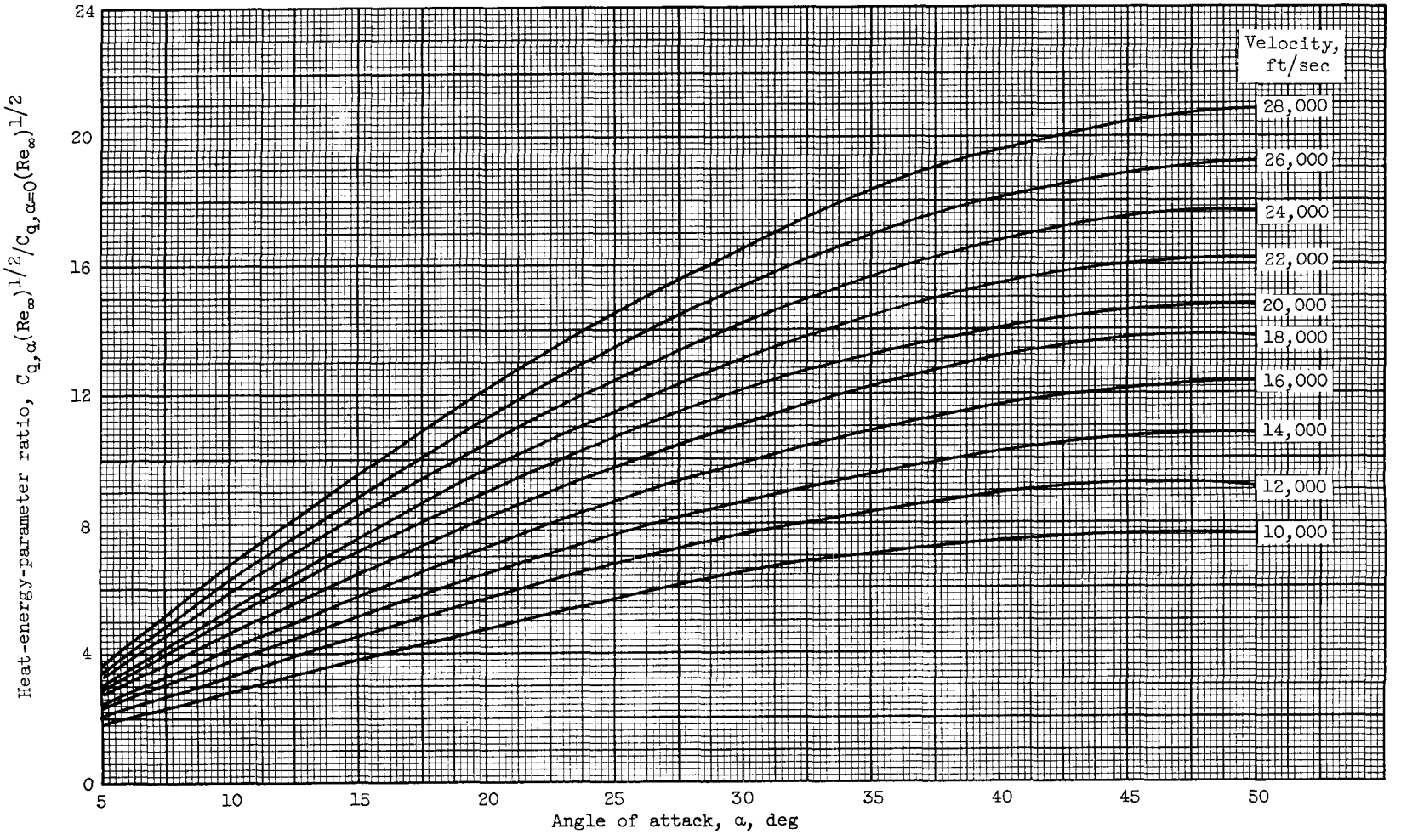

(e) Altitude, 250,000 feet.

Figure 13. - Continued. Effect of angle of attack on heat-energy-parameter ratio as a function of velocity. Wall temperature, T_w, 1000° R; laminar boundary layer.

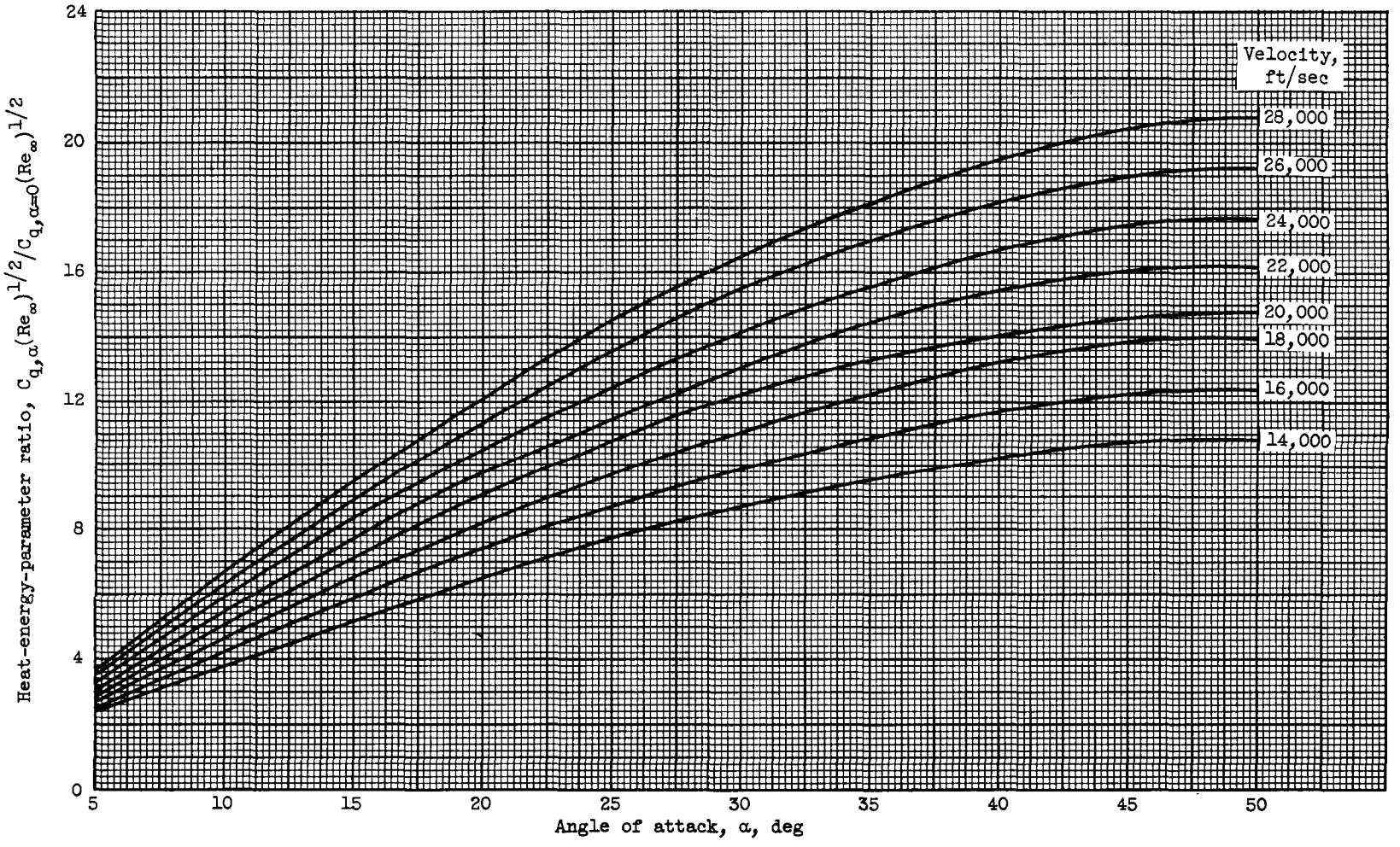

(f) Altitude, 300,000 feet.

Figure 13. - Concluded. Effect of angle of attack on heat-energy-parameter ratio as a function of velocity. Wall temperature, T_w, 1000° R; laminar boundary layer.

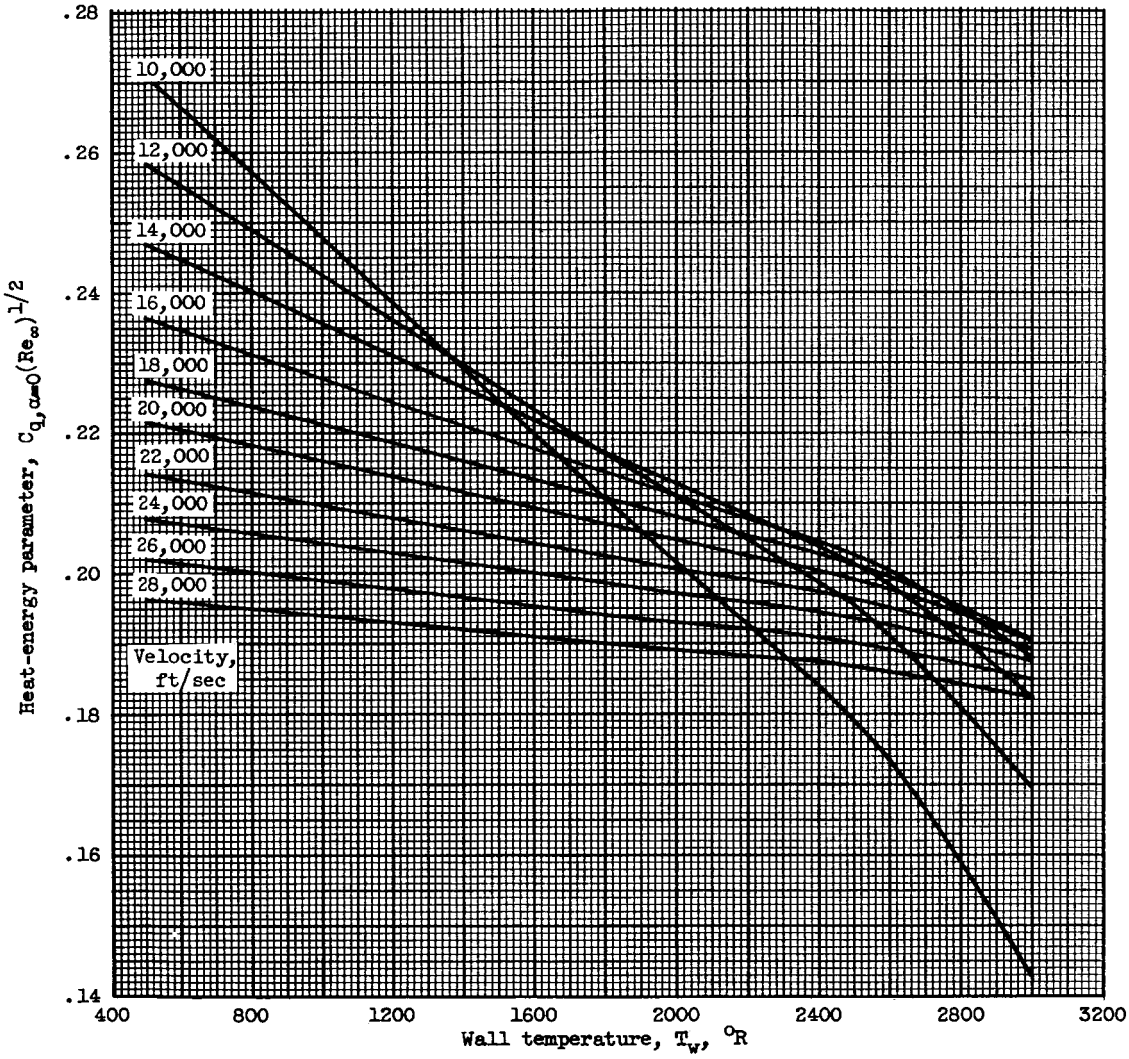

(a) Altitude, 50,000 feet.

Figure 14. - Effect of wall temperature on heat-energy parameter at zero angle of attack. Laminar boundary layer.

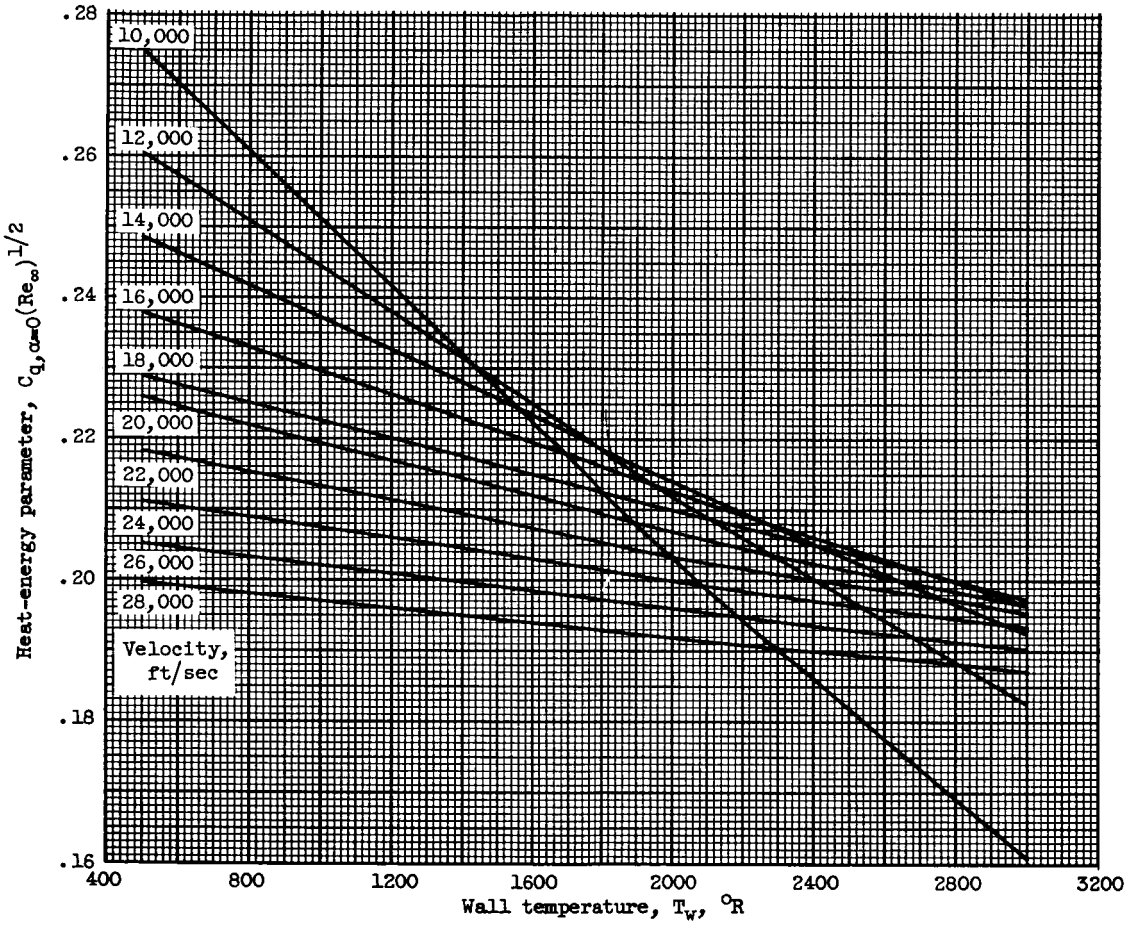

(b) Altitude, 100,000 feet.

Figure 14. - Continued. Effect of wall temperature on heat-energy parameter at zero angle of attack. Laminar boundary layer.

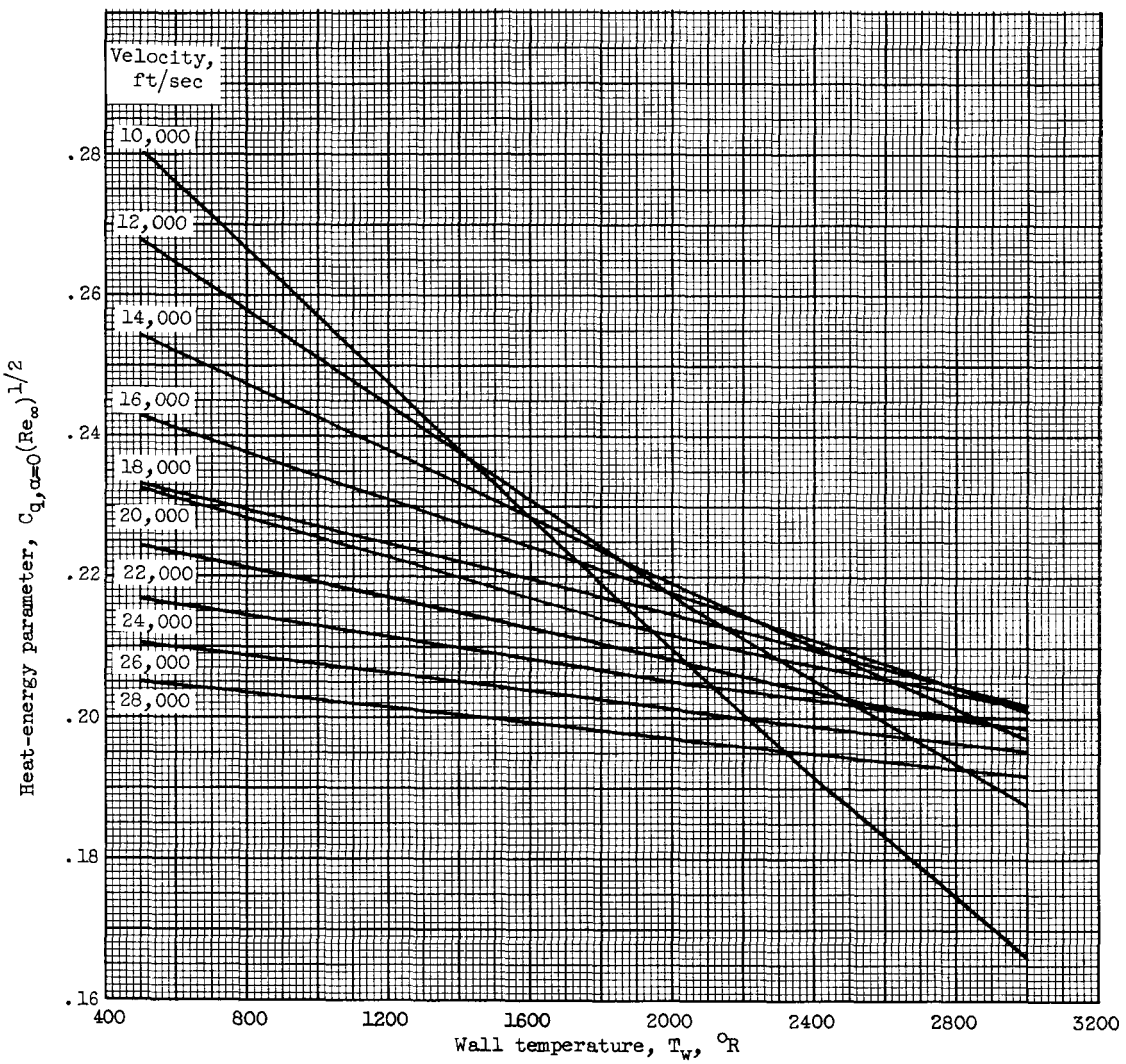

(c) Altitude, 150,000 feet.

Figure 14. - Continued. Effect of wall temperature on heat-energy parameter at zero angle of attack. Laminar boundary layer.

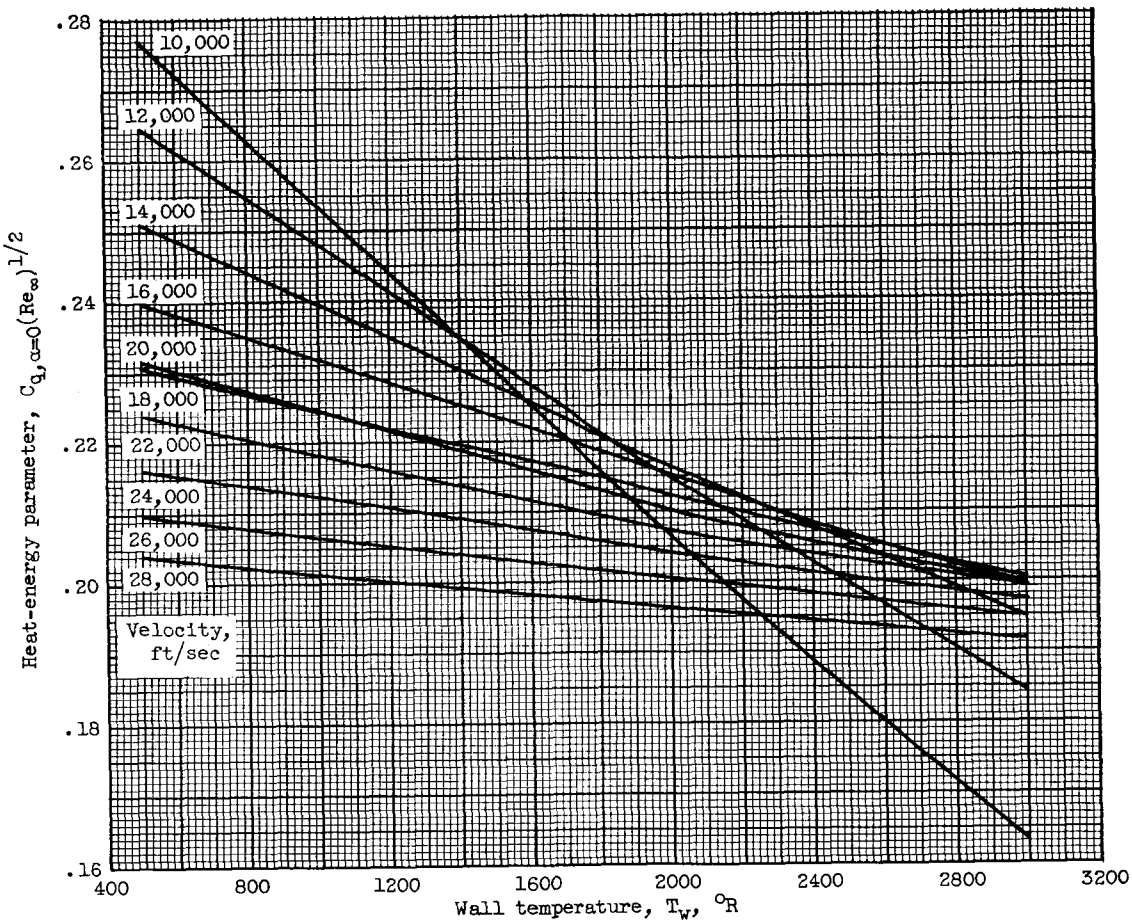

(d) Altitude, 200,000 feet.

Figure 14. - Continued. Effect of wall temperature on heat-energy parameter at zero angle of attack. Laminar boundary layer.

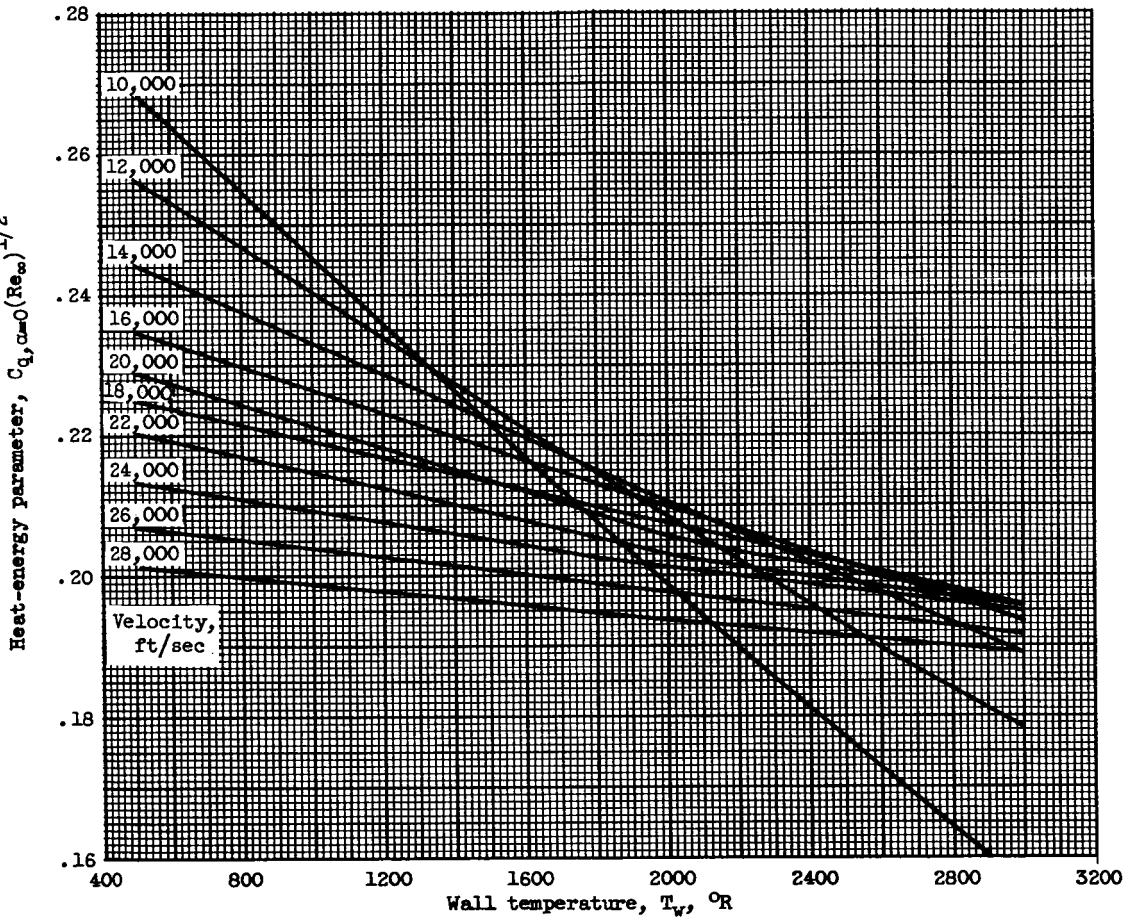

(e) Altitude, 250,000 feet.

Figure 14. - Continued. Effect of wall temperature on heat-energy parameter at zero angle of attack. Laminar boundary layer.

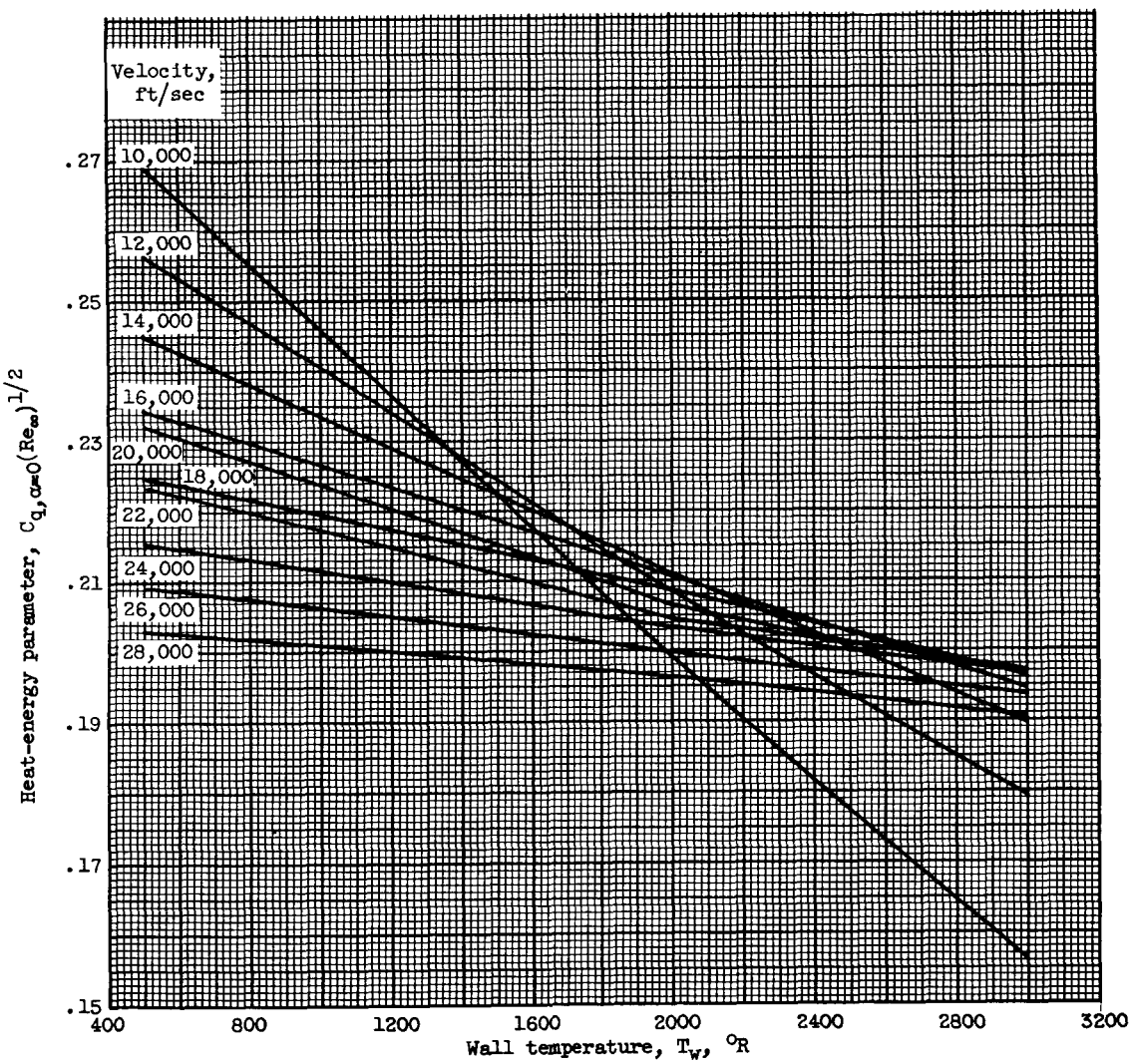

(f) Altitude, 300,000 feet.

Figure 14. - Concluded. Effect of wall temperature on heat-energy parameter at zero angle of attack. Laminar boundary layer.

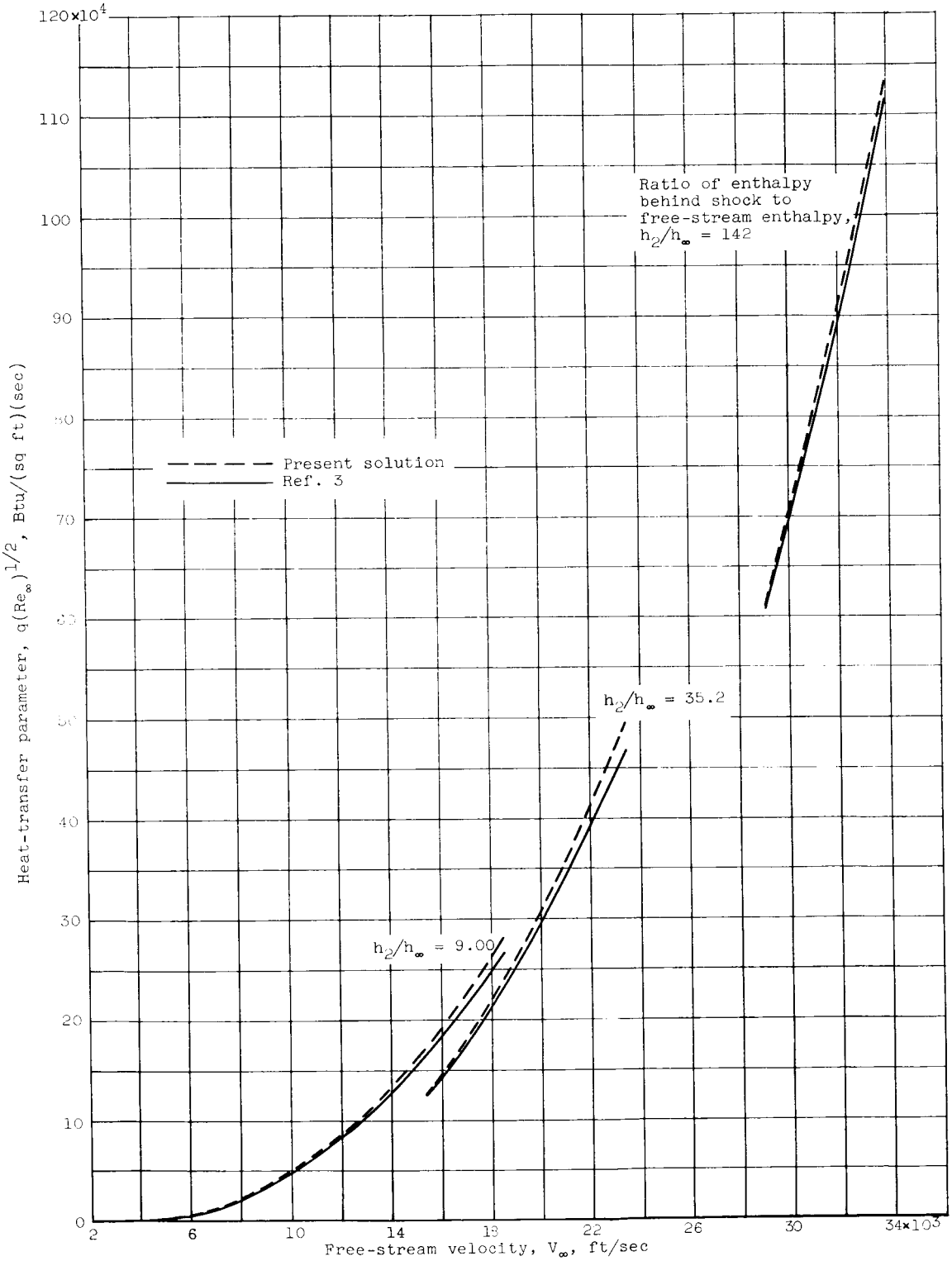

Figure 15. - Comparison of the present solution with the method of reference 3 for the laminar heat-transfer rate. Wall temperature, 1000° R; dissociation equilibrium pressure, 1 atmosphere; laminar boundary layer.

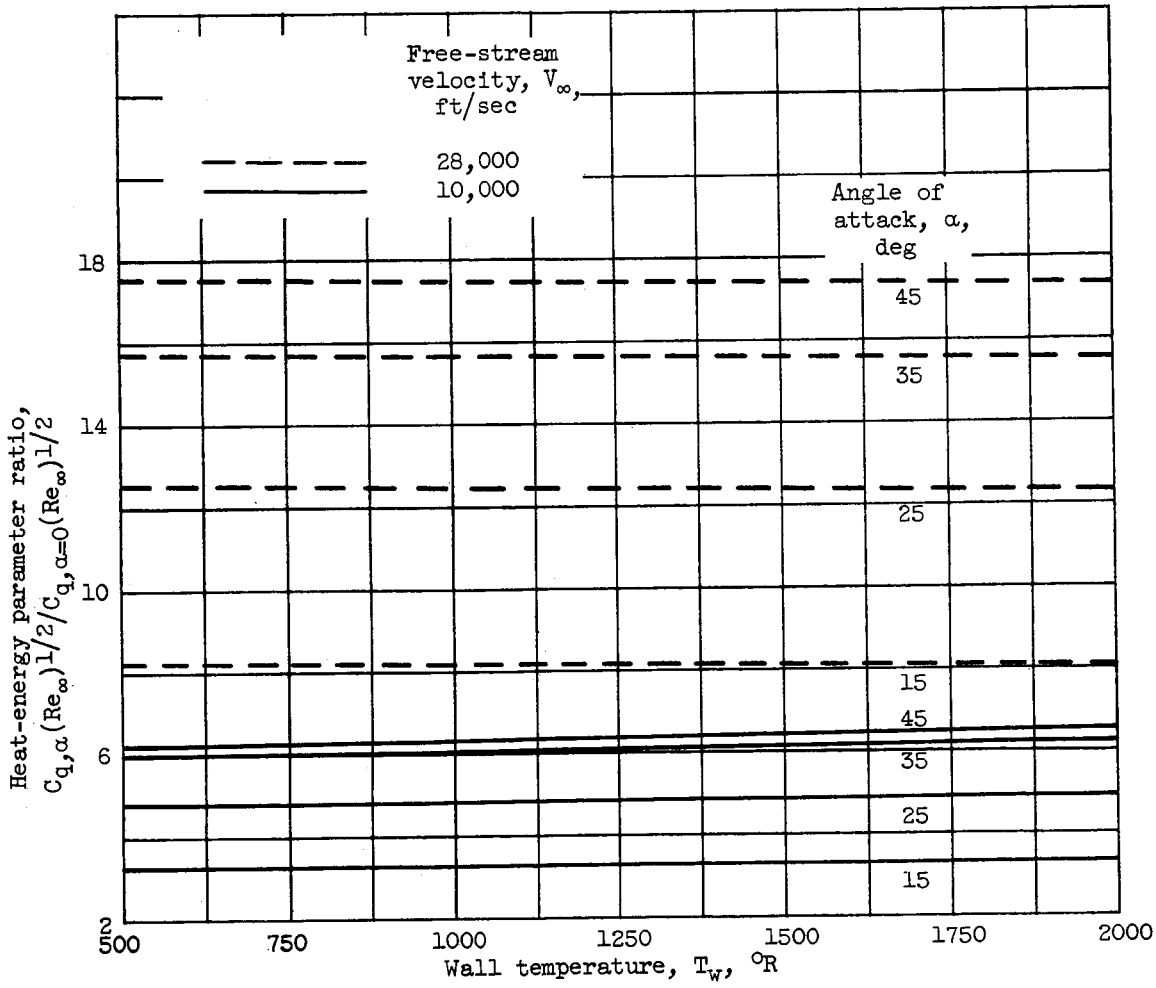

Figure 16. - Effect of wall temperature on laminar heat-energy parameter ratio as a function of angle of attack. Altitude, 150,000 feet; laminar boundary layer.